Nonlinear Oscillations of Self-Excited Systems Under Multifrequency Parametric Excitation

by

Wafa Limam

Thesis submitted to the Faculty of the

Virginia Polytechnic Institute and State University

in partial fulfillment of the requirements for the degree of

Master of Science

in

Civil Engineering

APPROVED:

Raymond H. Plaut, Chairman

Siegfried M. Holzer

Dean T. Mook

July 28, 1989

Blacksburg, Virginia

Nonlinear Oscillations of Self-Excited Systems Under Multifrequency Parametric Excitation

by

Wafa Limam

Raymond H. Plaut, Chairman

Civil Engineering

(ABSTRACT)

A self-excited system with weak nonlinearities and multifrequency parametric excitation is investigated in this study. The method of multiple scales is used to analyze the system under four different resonances relating parametric excitation frequencies with the natural frequencies. In the first case, the parametric excitation frequency is approximately equal to twice the natural frequency, $\lambda \simeq 2\omega$. In the second case, the parametric excitation frequency is approximately equal to the natural frequency, $\lambda \simeq \omega$. The third case treats a system with two parametric excitation frequencies under the condition $\lambda_2 \pm \lambda_1 \simeq 2\omega$. In the last case, a two-degree-of-freedom system with natural frequencies ω_q and ω_r is considered and the resonance $\lambda_1 + \lambda_2 \simeq \omega_r - \omega_q$ is analyzed. Different parameters (the load amplitudes, a detuning parameter, and a system stiffness parameter) are varied in each case and the responses obtained are presented in plots. The stability of the solutions is affected by all the parameters mentioned, especially the load amplitudes and the detuning parameter.

Acknowledgements

Dr. Plaut, thank you for being always so patient and so helpful. I thank my dear parents, and my sisters and my brothers for always believing in me and supporting me. Special thanks to a great bunch of people here in Blacksburg, and and I'll always remember all of you with very special thoughts. To all the friends I met in Blacksburg, thank you for being there.

I also want to acknowledge the U.S. Army Research Office for partial financial support of this research under grant no. DAAL03-87-K-0040.

Table of Contents

List of Illustrations

CHAPTER 1

1.1 INTRODUCTION

In this thesis we are looking into the behavior of a self-excited system under parametric excitation. In real life, some phenomena, man-made or natural, can induce the behavior of self-excited systems. One example is dry friction in the case of a mass sitting on a moving mat and attached to a fixed end (see Fig. 1.1). Another example of self-excited systems was introduced by Rayleigh when he explained the vibrations produced by drawing a bow across the string of a violin in one direction. A very important characteristic of self-excited systems is that the force exerted on the system is constant in one direction, and yet at a certain time the system exhibits vibrations.

As a reminder, the Tacoma-Narrows bridge failure was caused by flow-induced vibrations due to the wind. Self-excited oscillations in systems and structures can be dangerous; we need to control them, especially in structures such as skyscrapers, bridges, stacks, heat exchangers, etc.

When one tries to explain parametric excitations, one should start by saying that in mathematical terms this behavior appears in the governing equations of motion, of a structure or a system, as a time-varying coefficient. Different types of forces can produce this type of behavior. One example is the vertical component of an earthquake acting on a high-rise building; another simple example is an axially loaded column when the load oscillates. When not controlled, parametric excitations can cause instability of the structure.

Now that we have described parametric excitations and self-excited systems, and how dangerous they could be on structures, therefore on the occupants, we see how important it is to study these behaviors and investigate the factors affecting them. At this time, we would like to introduce the general governing equations of motion; they are assumed to have the form:

$$\begin{aligned}
&\ddot{u}_n + \omega_n^2 u_n + \varepsilon \sum_{j=1}^{N}\sum_{k=1}^{N} \Lambda_{jkn} u_j u_k + \varepsilon^2 \sum_{j=1}^{N}\sum_{k=1}^{N}\sum_{l=1}^{N} \Gamma_{jkln} u_j u_k u_l - 2\varepsilon^2 \sum_{j=1}^{N} B_{jn}\dot{u}_j \\
&+ \varepsilon^2 \sum_{j=1}^{N}\sum_{k=1}^{N}\sum_{l=1}^{N} C_{jkln} u_j u_k \dot{u}_l + \varepsilon^2 \sum_{j=1}^{N}\sum_{k=1}^{N}\sum_{l=1}^{N} D_{jkln}\dot{u}_j\dot{u}_k\dot{u}_l \qquad (1.1) \\
&+ 2\varepsilon \sum_{m=1}^{N} \cos(\lambda_m t + \tau_m) \sum_{j=1}^{N} Q_{jn}^{m}(\varepsilon) u_j = 0; \qquad n = 1,2,\ldots
\end{aligned}$$

For a single degree of freedom with single-frequency excitation, we can drop the subscripts and the superscripts and write the equation of motion as:

$$\ddot{u} + \omega^2 u + \varepsilon\Lambda u^2 + \varepsilon^2\Gamma u^3 - 2\varepsilon^2 B\dot{u} + \varepsilon^2 C u^2\dot{u} + \varepsilon^2 D\dot{u}^3 + 2\varepsilon\cos(\lambda t + \tau)Q(\varepsilon)u = 0 \quad (1.2)$$

where

$u(t)$ is the generalized coordinate,

$\dot{u}$ is the velocity,

$\ddot{u}$ is the acceleration,

ω is the natural frequency of the system,

B , C, and D are constant coefficients of the velocity-dependent terms,

ε is a small parameter,

Q, λ, and τ are the amplitude, frequency and phase of the parametric excitation, respectively,

and

Λ and Γ are constant coefficients of the nonlinear terms in the system stiffness.

A special case of equation (1.2) when we have $B > 0$, $C > 0$, $D = 0$, $\Lambda = 0$, $\Gamma = 0$, and $Q = 0$ is the van der Pol equation:

$$\ddot{u} + \omega^2 u - 2\varepsilon^2 B\dot{u} + \varepsilon^2 C u^2\dot{u} = 0. \quad (1.3)$$

Another special case, the Rayleigh equation, occurs for $B > 0$, $C = 0$, $D > 0$, $\Lambda = 0$, $\Gamma = 0$, and $Q = 0$:

$$\ddot{u} + \omega^2 u - 2\varepsilon^2 B\dot{u} + \varepsilon^2 D\dot{u}^3 = 0. \quad (1.4)$$

1.2 LITERATURE REVIEW

Parametric excitation and self-excited systems have been the center of interest for a number of researchers. Many investigations have been carried out to get a better understanding of these two types of behavior. However, most of the time, researchers have only taken an interest in either parametric excitation or self-excited systems. Only a few have looked at these behaviors acting together on a system.

As we will see in the following discussion, different researchers have used different methods of solution. They have also treated different types of parametric resonance. As a matter of fact, most of the studies have considered the case where the frequency of the parametric excitation is approximately equal to twice the natural frequency of a single-degree-of-freedom system, $\lambda \simeq 2\omega$.

Kononenko and Koval'chuk [1] have discussed the effect of parametric excitation on a self-oscillatory system. They only treated a single-degree-of-freedom system with the parametric frequency approximately equal to twice the natural frequency, $\lambda \simeq 2\omega$. These two researchers have also presented a study on the effect of an external harmonic force on a self-excited oscillating system with a variable parameter [2]. They have studied the special case of a van der Pol equation and again the parametric resonance was taken equal to twice the natural frequency, $\lambda \simeq 2\omega$.

Tondl [3] has written a report on the interaction between self-excited and parametric vibrations in which he analyzed the problem in a little more general way. Even though Tondl considered a slightly different system and his method of solving the problem was

different, we find some similarities in his results and ours, especially in the case of linear stiffness and for a perfectly tuned system, $\lambda = 2\omega$.

The special case of Rayleigh's equation with principal parametric excitation, $\lambda \simeq 2\omega$, was analyzed by Nayfeh and Mook [4] in an example in their Nonlinear Oscillations book (pp. 342-343).

In a series of papers, Yano [5-10] has considered parametric excitation in self-excited systems. First, he analyzed a single-degree-of-freedom system with dry friction and with the parametric frequency approximately equal to twice the natural frequency, $\lambda \simeq 2\omega$ [5]. He used different methods of solution, the averaging and the numerical integration methods, and yet we find some similarities in the system responses. The first report was followed by a second one on the same subject [6]. In a third paper [7], he treated parametric excitation in a self-excited vibration system, discussing the influence of a cubic nonlinearity on the system. In that paper he considered three different cases of parametric resonance: when the parametric frequency is twice the natural frequency, $\lambda \simeq 2\omega$, then approximately equal to the natural frequency, $\lambda \simeq \omega$, and the last case, when it is four times the natural frequency, $\lambda \simeq 4\omega$. Here again we find a lot of similarities in the graphs representing the responses for the $\lambda \simeq 2\omega$ case with our results. In references [8-10] by Yano, the problem analyzed was different and in each report the parametric resonances considered were different. In the first one [8], he was interested in the region of subharmonic resonance when $\lambda \simeq 4\omega$, as well as the case when $\lambda \simeq 2\omega$. The second report [9] discussed the van der Pol special case and the behaviors when the resonances are respectively $\lambda \simeq \omega$ and $\lambda \simeq 6\omega$, and again there are similarities in the responses he presented for $\lambda \simeq \omega$ and the ones we obtain. His third report [10] dealt with the resonance when $\lambda \simeq 3\omega$.

Yano has also joined efforts with other researchers who shared his interest in these types of behavior. In 1985, Kotera and Yano published a paper [11] on a system which was similar to Tondl's and Yano's. The parametric frequencies were taken to be equal to the natural frequency or equal to twice the natural frequency.

On parametric excitation with an asymmetric characteristic in a self-exciting system, Yano, Kotera, and Hiramatsu [12] discussed a system with the parametric frequency equal to the natural frequency, $\lambda \simeq \omega$. In another paper [13], the three authors used both the method of averaging and the method of harmonic balance for the case when the parametric frequency is equal to twice the natural frequency. Another investigation was carried out by Schmidt and Tondl [14], in their Nonlinear Vibrations book, dealing with the van der Pol special case. They treated the case with the parametric resonance equal to twice the natural frequency, $\lambda \simeq 2\omega$, and again we mention the close similarities we find in the responses obtained.

In his dissertation, Asfar [15] has analyzed the response of self-excited multi-degree-of-freedom systems to multifrequency external excitations. He only took self-excited systems into account and did not look into the influence of parametric excitation.

Other researchers, such as Weidenhammer [16], Nayfeh and Jebril [17], Othman and Watt [18], Plaut [19], and Plaut, Gentry, and Mook [20] have been interested in nonlinear oscillations under multifrequency parametric excitation, but did not discuss self-excited systems in their respective papers.

1.3 THE PRESENT STUDY

The method of multiple scales is used throughout the analysis to solve the governing equations of motion and to give us certain resonances of interest to investigate.

In this thesis, four types of resonances are investigated. The results are presented for each case in the form of different plots. We first look into the case where the frequency of the parametric excitation is approximately equal to twice the natural frequency of the system, $\lambda \simeq 2\omega$. The system is analyzed and some factors like the detuning parameter, σ, the loading amplitude, P, and a measure of the nonlinearity of the stiffness, α, are varied to check their influence on the system response, or more precisely, the amplitude of the response, a. These responses are plotted in graphs showing a vs. P and a vs. σ.

The second case occurs when the frequency of the parametric excitation is approximately equal to the natural frequency of the system, $\lambda \simeq \omega$. The same analysis is performed and the same factors are investigated. The responses are also presented graphically.

In the third case, we consider two parametric excitations acting on the system. We have two frequencies and two load amplitudes to deal with. The resonance we examine is when the sum or the difference of these two frequencies is approximately equal to twice the natural frequency, $\lambda_2 \pm \lambda_1 \simeq 2\omega$. Again, similar investigations to the other two cases are performed and similar types of graphs are presented to show the responses obtained.

Finally, in the last case, we treat a two-degree-of-freedom system and we include the two parametric excitations. There are two natural frequencies, ω_r and ω_q. The case we study is when the sum of the two excitation frequencies is approximately equal to the difference of the natural frequencies, $\lambda_1 + \lambda_2 \simeq \omega_r - \omega_q$.

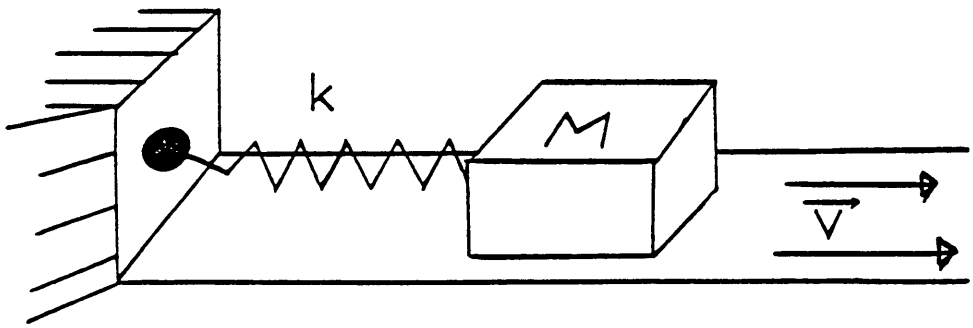

Figure 1. Mass Attached to a Spring on a Moving Mat: An Example of Dry Friction on Self-Excited Systems.

CHAPTER 2

CASE ONE : $\lambda \simeq 2\omega$

We start the research by investigating the case when the frequency of the parametric excitation is approximately equal to twice the natural frequency, $\lambda \simeq 2\omega$. As mentioned in the literature review, this case was treated by many reseachers, but no one has yet analyzed the exact same system as the one we are investigating.

The governing equation of motion, when we have a single degree of freedom and a single-frequency excitation, is of the form :

$$\begin{aligned} &\ddot{u} + \omega^2 u - 2\varepsilon^2 B\dot{u} + \varepsilon\Lambda u^2 + \varepsilon^2 \Gamma u^3 \\ &\quad + \varepsilon^2 C u^2 \dot{u} + \varepsilon^2 D\dot{u}^3 + 2\varepsilon \cos(\lambda t + \tau) Q(\varepsilon) u = 0 \end{aligned} \tag{2.1}$$

For $\lambda \simeq 2\omega$, we let $Q = 2\varepsilon\omega P$ and equation (2.1) becomes

$$\begin{aligned} &\ddot{u} + \omega^2 u - 2\varepsilon^2 B\dot{u} + \varepsilon^2 \Lambda u^2 + \varepsilon^2 \Gamma u^3 \\ &\quad + \varepsilon^2 C u^2 \dot{u} + \varepsilon^2 D\dot{u}^3 + 4\varepsilon^2 \omega P u \cos(\lambda t + \tau) = 0 \end{aligned} \tag{2.2}$$

We assume that $B > 0$, $C \geq 0$, and $D \geq 0$, with either C or D (or both) positive.

The method of multiple scales [4] is used to analyze the system and to obtain an approximate solution to the nonlinear equation. The general form of the solution is:

$$u(t) = a\cos(\omega t + \beta) + \varepsilon u_1(t) + \varepsilon^2 u_2(t) + \cdots \tag{2.3}$$

where a is the amplitude of the lowest-order term and β is the phase. In this chapter we are assuming that

$$\lambda = 2\omega + \varepsilon^2 \sigma \tag{2.4}$$

where σ is the detuning parameter.

From the method of multiple scales, we get a relationship between the amplitude of the response, a, the load amplitude, P, and the detuning parameter, σ. We are only looking at steady-state solutions. In this case,

$$a^2 = \frac{2B\xi - \sigma\alpha \pm 2\sqrt{P^2\alpha^2 - B^2\alpha^2 + P^2\xi^2 - \dfrac{\sigma^2\xi^2}{4} - B\xi\sigma\alpha}}{2(\xi^2 + \alpha^2)} \tag{2.5}$$

where $\xi > 0$ and has the form:

$$\xi = \frac{1}{8}(C + 3\omega^2 D) \tag{2.6}$$

and α the stiffness of the system has the following formula:

$$\alpha = -\frac{3}{8}\frac{\Gamma}{\omega} + \frac{5}{12}\frac{\Lambda}{\omega^3} \tag{2.7}$$

In all our cases α will be either -1, 0, or 1. For simplification we set $\xi = 1$ and $B = 1$. We have a steady-state trivial solution, $a = 0$, and other real solutions when a^2 is real and positive ($a^2 > 0$) in (2.5).

The stability of steady-state solutions is determined in the usual manner [4]. We consider small motions about the steady state and see whether or not they can grow large. In the plots, solid lines denote stable solutions and dashed lines represent unstable solutions.

We first consider Fig. 2.1. It shows how many steady-state solutions exist for different combinations of the detuning parameter, σ, and the load amplitude, P. In each plot of Fig. 2.1 these regions of existence are outlined by the staight lines and the hyperbola. The straight lines come out of the following formula for P:

$$P = \frac{\pm \left| B\alpha + \frac{\xi\sigma}{2} \right|}{\sqrt{\xi^2 + \alpha^2}} \tag{2.8}$$

and the hyperbola by:

$$P = \sqrt{B^2 + \frac{\sigma^2}{4}} \tag{2.9}$$

Now we go back to Fig. 2.1 and check those regions of existence we are referring to. The region marked I on the graph is where no other solution exists besides the trivial solution, $a = 0$. Region II is where two solutions exist; the trivial solution is one and the second one is a nontrivial solution. In the region marked III we have two nontrivial solutions besides the trivial one. Another parameter affecting these regions of existing solutions is the stiffness α; this parameter is zero when the stiffness is linear ($\Lambda = 0, \Gamma = 0$). Negative stiffness, in our case $\alpha = -1$, is when the system is hardening, and this affects the solution by having the boundaries of region I move to the right in the graph (see Fig 2.1a). When the system is softening, meaning the stiffness is positive, and in our study $\alpha = 1$, the boundaries of region I move to the left in the graph as seen in Fig. 2.1c. This right and left movement of the solutions is a trend that keeps occurring any time the stiffness is varied from zero to -1 or 1. Looking at these graphs again, we notice that region II is not affected by the stiffness in any case, while region III where two real positive solutions exist is really affected by the linearity or nonlinearity of the system stiffness. When $\alpha = 0$, the range of solutions is very small; this range gets wider with absolute values of α larger than zero. We note that Fig. 2.2 explains to the reader what is happening in the system when the stiffness is negative, zero or positive, where the F on the graph represents the elastic restoring force of the system.

Figure 2.3 shows the response amplitude, a, versus the load, P. It is obvious as we look at the graphs that as the P value gets larger, the stable nontrivial response amplitude, a, gets larger. The three different curves represent three different cases of the detuning parameter, σ. The first curve, the one touching the vertical axis, is the $\sigma = 0$ case; the system is perfectly tuned. As the detuning parameter gets larger, the bifurcation load at which the system changes from being unstable to stable gets larger and the response amplitude, a, goes down, which is expected.

As explained earlier in this chapter, the dashed and solid lines in the figures refer to the solution being unstable and stable, respectively. There is a small remark to make about the way we show stability and instability for the steady-state trivial solution, $a = 0$. Since we have more than one response curve plotted in one graph, and because the trivial solution is only unstable until the bifurcation point of the respective curve, we have only marked instability until the first bifurcation point. Therefore, we have to remember that for the second curve on the graph, for example, the trivial solution is unstable until the second bifurcation point, which corresponds to that response curve.

Figure 2.4 is related to Fig. 2.3 in that they both represent the change in the response amplitude versus the change in the load amplitude. The difference, though, is in the system stiffness. While Fig. 2.3 shows the response of the system for linear stiffness ($\alpha = 0$), Fig. 2.4 corresponds to the system with nonlinear stiffness ($\alpha \neq 0$). In Figs. 2.4a and 2.4b we set the detuning parameter equal to zero ($\sigma = 0$) and unity ($\sigma = 1$), respectively, and we check the effect of varying the stiffness value α. When $\sigma = 0$, a perfectly tuned system, in Fig. 2.4a we see the same curve as in Fig. 2.3 for $\alpha = 1$. Then for $\alpha = 1$ or $\alpha = -1$, which have the same response, the amplitude, a, is much smaller. Even though they have the same bifurcation point, the load at which nontrivial solutions begin to exist is larger for $\alpha \neq 0$. As far as Fig. 2.4b is concerned, again we see the same curve as in Fig. 2.3 for $\sigma = 1$ and $\alpha = 0$, and we also notice the effect of nonlinear stiffness on the system response. Both responses have smaller amplitudes as the load gets larger, and they all have the same bifurcation point, which tells us that the trivial solution is stable for any system stiffness in a certain range of load amplitudes, P. However, when it comes to the nontrivial solutions, the load at which the response begins to exist is greatly affected by the system stiffness. When $\alpha = 1$, this load is much larger than when $\alpha = 0$ or $\alpha = -1$.

Moving on to Fig. 2.5, we see that the plot corresponds to the response amplitude a versus the detuning parameter σ. We are first checking a linear stiffness system, $\alpha = 0$, and varying the load amplitude, P. As P gets larger, the response gets larger, too. Also, for $a > 1$, all the different solutions are stable. Again we mention the way that the trivial solution stability is marked. For the cases $P = 0.5$ and $P = 1.0$ the trivial solution is always unstable; for the case $P = 1.5$, we have two bifurcation points and the trivial solution is only stable between these points.

Basically, looking at Figs. 2.6(a,b,c,d) is the same as looking at Fig. 2.5 with small changes in the parameters. It also shows how the response amplitude increases, and the range of stable solutions increases, as the load P increases. What we are trying to present in all of the plots in Fig. 2.6 is again how the system is affected by the stiffness parameter α defined in equation (2.9).

In each case we set the value of α. The response plotted in the middle of each graph represents the linear stiffness case, $\alpha = 0$. The response on the right is for $\alpha = -1$ and the one on the left of the graph is for $\alpha = 1$. It is noticeable that the size of the response is not affected much by α . However, the range of the detuning parameter at which the responses are stable is different for each case. We see that the ranges overlap, and seem to get larger as P increases. In this particular figure the trivial solution stability or instability is shown clearly and actually explains a little bit how the other figures have been marked. As mentioned earlier in the literature review, we find a lot of similarities between these figures presented in this chapter and the figures presented by different authors in their discussions of this case, $\lambda \simeq 2\omega$. In particular, the $P = 1$ case of Fig. 2.5, although not complete, was given in the example discussed in the Nayfeh and Mook book [4, p.342]. Also, curves similar to those for $\sigma = 0$ in Fig. 2.3, $P = 0.5$ in Fig. 2.5,

and $\alpha = 0$ and -1 in Fig. 2.6d were given in [14, p.139], [14. p.140], and [3, p.15], respectively.

At the end of this chapter, we conclude by reminding the reader that in the $\lambda \simeq 2\omega$ case we studied the changes in the system as we varied the system stiffness value, α, or the load amplitude, P, or the detuning parameter, σ. As we can expect, for larger values of P, the response tends to increase. To the contrary, for larger magnitudes of the detuning parameter, σ, the response tends to decrease if $\alpha = 0$ until only the trivial solution exists. If $\alpha \neq 0$ and σ is increased in magnitude, the stable nontrivial steady-state amplitude first increases, then decreases, and then ceases to exist.

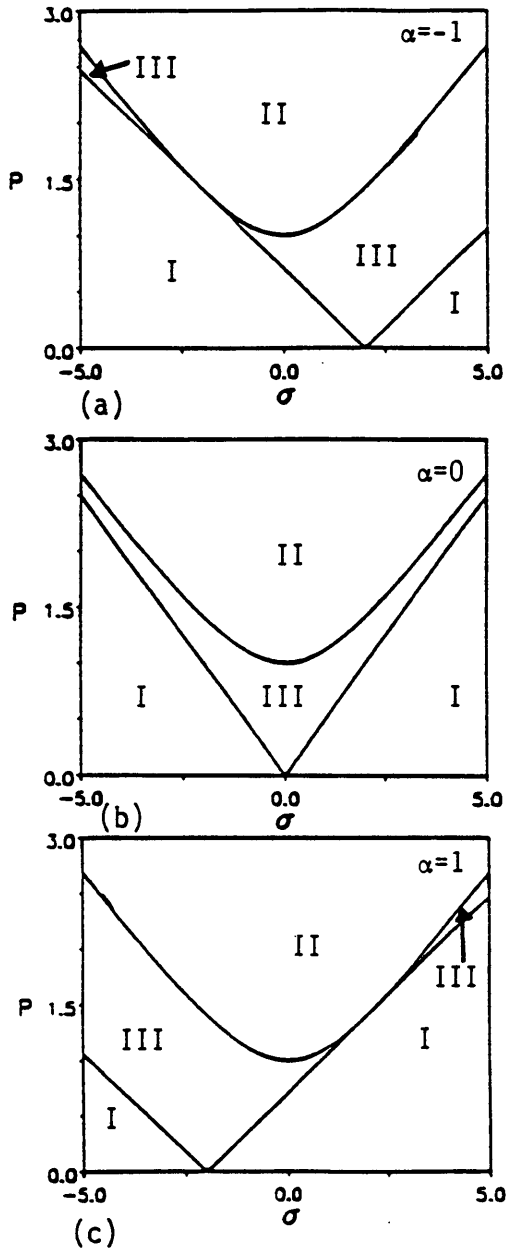

Figure 2.1. Regions of Existing Solutions, P vs. σ

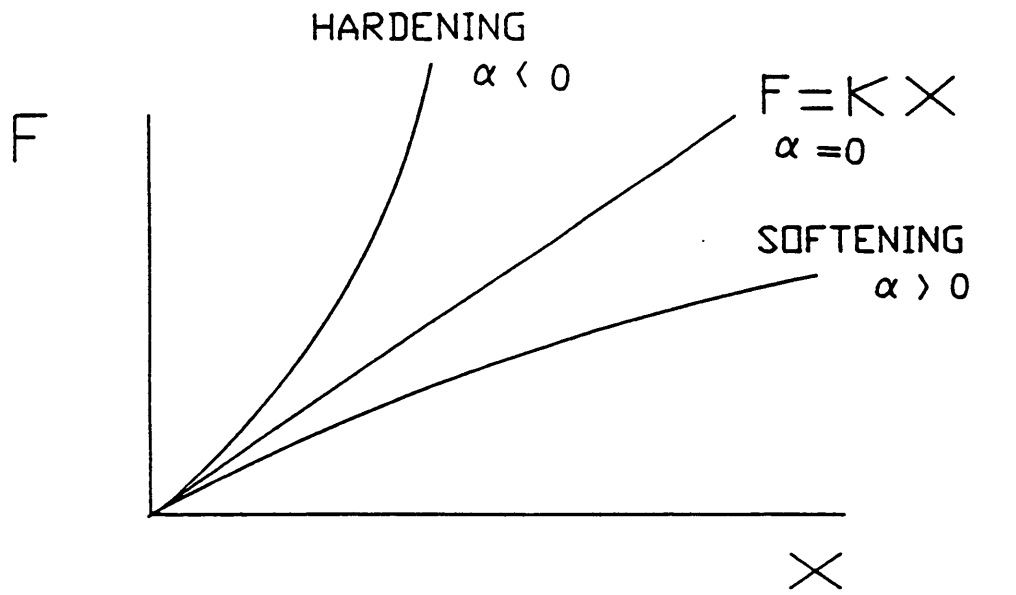

Figure 2.2. A Measure of the System Stiffness.

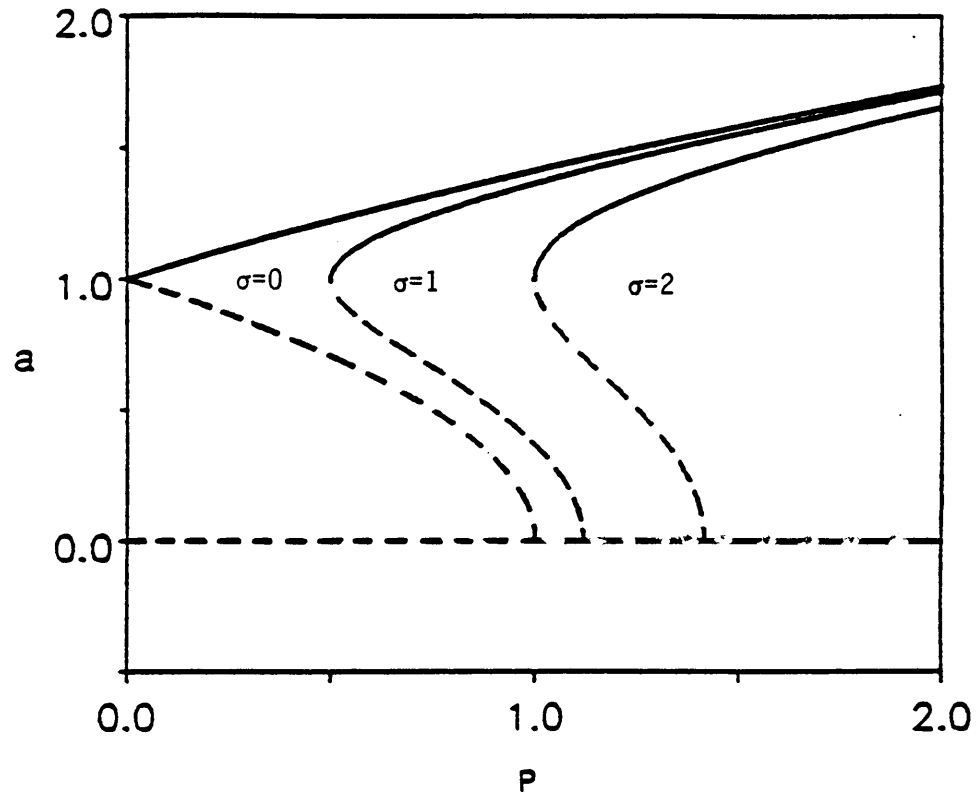

Figure 2.3. The Response Amplitude Versus The Load Amplitude, a vs. P .

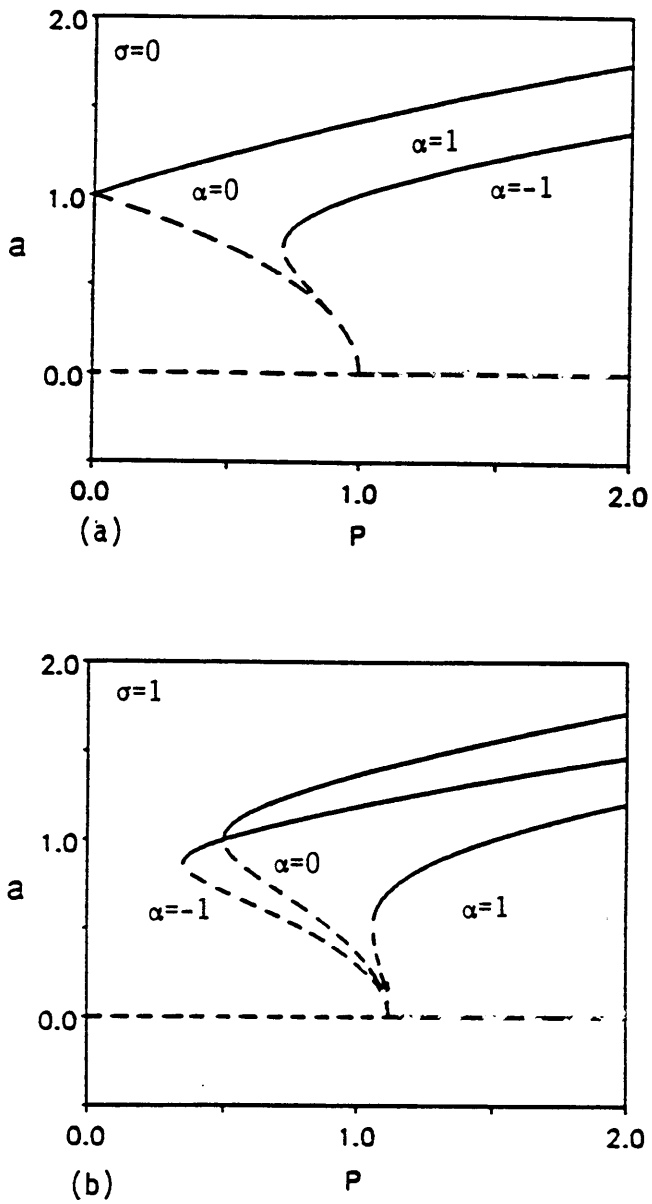

Figure 2.4. The Response Amplitude Versus The Load Amplitude, a vs. P .

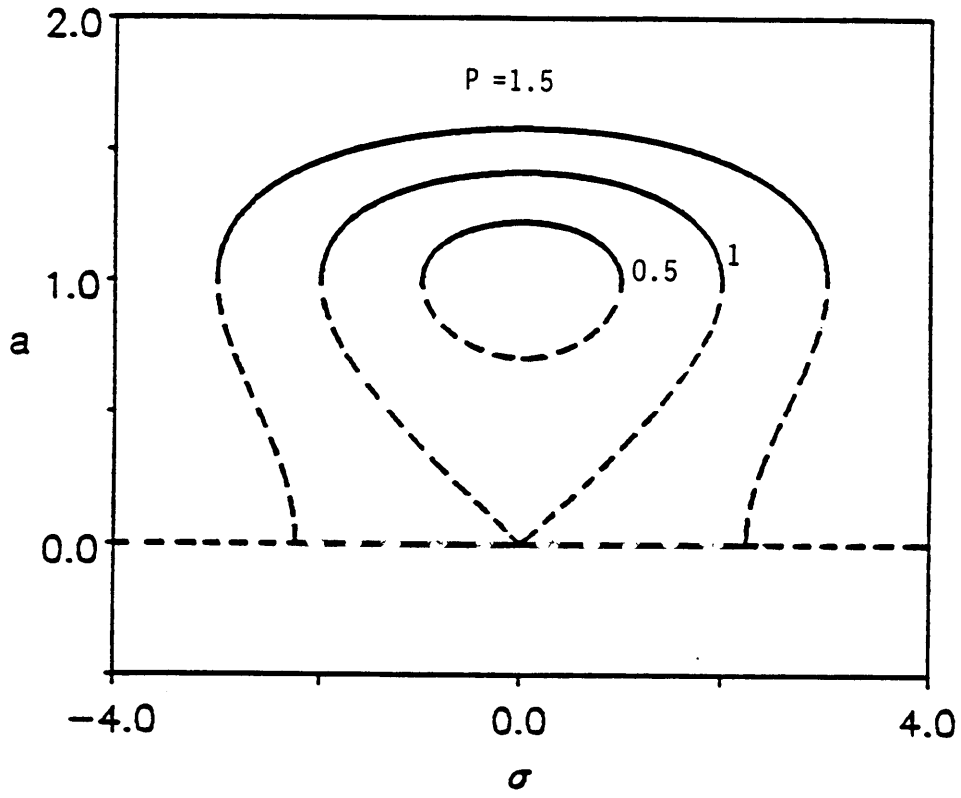

Figure 2.5. **Frequency-Response Curves, a vs. σ .**

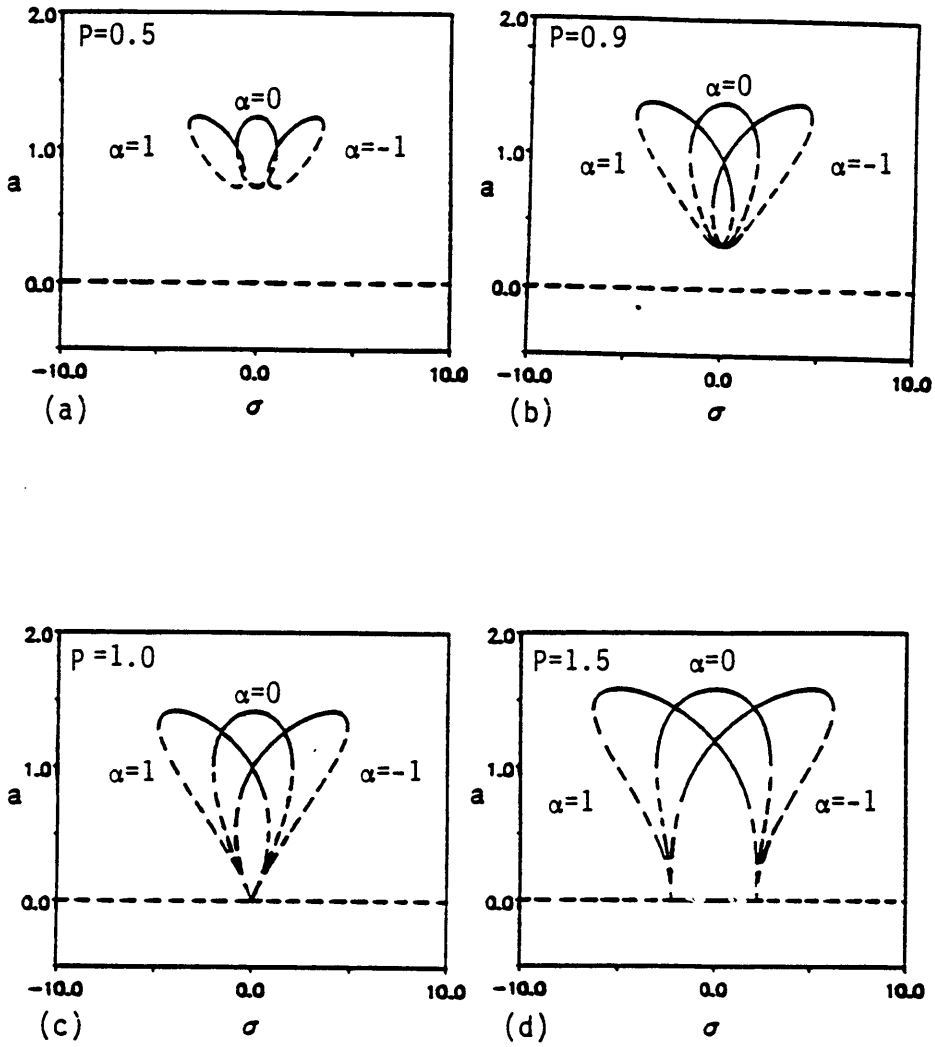

Figure 2.6. Frequency-Response Curves, a vs. σ .

CHAPTER 3

CASE TWO : $\lambda \simeq \omega$

In this chapter we consider the case where the frequency of the parametric excitation is approximately equal to the natural frequency of the system. Again we are looking at the same nonlinear equation (2.1) presented in chapter 2, for a single-degree-of-freedom system with a single-frequency excitation. When

$$\lambda = \omega + \varepsilon^2 \sigma \tag{3.1}$$

and

$$Q = 2\omega P \tag{3.2}$$

equation (2.1) becomes:

$$\ddot{u} + \omega^2 u - 2\varepsilon^2 B\dot{u} + \varepsilon\Lambda u^2 + \varepsilon^2\Gamma u^3 + \varepsilon^2 C u^2\dot{u} + \varepsilon^2 D\dot{u}^3 + 4\varepsilon\omega u P\cos(\lambda t + \tau) = 0 \tag{3.3}$$

We solve the system with the method of multiple scales [4].

For the case of linear stiffness, the system response amplitude, a, is given by the following formula:

$$a^2 = \frac{1}{\xi}\left[B \pm \frac{1}{3}\sqrt{(10P^2 + 3\sigma)(2P^2 - 3\sigma)}\,\right] \tag{3.4}$$

It is assumed that $\xi > 0$ and $B > 0$.

We first determine the regions of existence of solutions, taking $\alpha = 0$ and $B = 1$. Fig. 3.1 shows the load amplitude, P, versus the detuning parameter, σ. As before, regions I, II and III are marked in the figure, and region I is where we only have the trivial solution, $a = 0$. Region II is where there is a nontrivial solution besides the $a = 0$ solution. Region III is where we find two nontrivial solutions besides $a = 0$. The curve between region II and III is given by the following formula:

$$\sigma = \frac{1}{3}\left(-4P^2 \pm 3\sqrt{4P^4 - B^2}\,\right) \tag{3.5}$$

while the left side of the curve dividing regions I and II is given by:

$$\sigma = -\frac{10}{3}P^2 \tag{3.6a}$$

and the right side by

$$\sigma = \frac{2}{3} P^2 \tag{3.6b}$$

For the nonlinear stiffness case, we have a system of two equations:

$$\begin{aligned} -B + \xi a^2 - C \sin 2\gamma - (2J - L)a \sin \gamma = 0 \\ \sigma - e + \alpha a^2 + C \cos 2\gamma + (2J + L)a \cos \gamma = 0 \end{aligned} \tag{3.7}$$

where

$$e = -\frac{4}{3} P^2,$$

$$\alpha = -\frac{3}{8} \frac{\Gamma}{\omega} + \frac{5}{12} \frac{\Lambda}{\omega^3},$$

$$C = 2 \frac{P^2}{\omega},$$

$$J = \frac{5\Lambda P}{6\omega^2},$$

and

$$L = J$$

We first set $\Lambda = 0$, which makes $J = L = 0$, and eliminate γ using $\cos^2 2\gamma + \sin^2 2\gamma = 1$. This gives the following formula for the system response amplitude:

$$a^2 = \frac{B\xi - (\sigma - e)\alpha \pm \sqrt{C^2\alpha^2 - B^2\alpha^2 + C^2\xi^2 - (\sigma - e)^2\xi^2 - B\xi\sigma\alpha}}{(\xi^2 + \alpha^2)} \tag{3.8}$$

We assume $\xi = 1$, $B = 1$, and $\omega = 1$.

Now we consider how the stability of the system in the $\lambda = \omega$ case has been examined. First, for any value of the response amplitude, a, that satisfies

$$a < \sqrt{\frac{B}{2\xi}} \tag{3.9}$$

the system is unstable. Next, we have to compute the following quantities:

$$C_1 = 2\xi a^2 - La \sin \gamma \tag{3.10}$$

$$C_2 = -2Ca \cos 2\gamma - La^2 \cos \gamma \tag{3.11}$$

$$C_3 = -2\alpha a - 3L \cos \gamma \tag{3.12}$$

$$C_4 = -2B + 2\xi a^2 + La \sin \gamma \tag{3.13}$$

Then we compute the quantity D, which dictates whether the system is stable or not:

$$D = C_1C_4 - C_2C_3 \tag{3.14}$$

If $D > 0$ and equation (3.9) is not satisfied, the system is stable; otherwise it is unstable. Again we remind the reader that dashed lines on the figures imply the system is unstable in that particular range of values of a, P, or σ. In Figs. 3.2, 3.3, and 3.4 it is easy to notice that at the vertical tangents of each curve the system response changes from being stable to unstable or vice versa.

Fig. 3.2 shows the response amplitude, a, versus the detuning parameter, σ, given by equation (3.8). The three different plots in the figure refer to the three cases of the system stiffness, $\alpha = -1$, 0, and 1, respectively. Again we see the trend that the shapes of the solutions follow when α is varied. We also see how the load P affects the system, which reacts with a larger response when P increases. As for the stability of these plotted responses, we notice that the stability range gets larger with larger responses due to larger load amplitudes applied to the system.

In Figs. 3.3 and 3.4 we also show the response amplitude, a, versus the detuning parameter, σ. Fig. 3.3 is for the case $\alpha = -1$ and Fig. 3.4 shows the responses when $\alpha = 1$. In these two figures we are dealing with the case where

$$\Lambda \neq 0\,, \quad B = 1, \quad \xi = 1, \quad \omega = 1,$$

$$J = L = \frac{5}{6}\Lambda P,$$

and

$$C = 2P^2$$

which makes the system of nonlinear equations (3.7) of the form:

$$\begin{cases} -1 + a^2 - 2P^2 \sin 2\gamma - \frac{5}{6}\Lambda P a \sin\gamma = 0 \\ \sigma + \frac{4}{3}P^2 + \alpha a^2 + 2P^2 \cos 2\gamma + \frac{5}{2}\Lambda P a \cos\gamma = 0 \end{cases} \tag{3.15}$$

Solving the first equation for a, we get:

$$a = \frac{5}{12}\Lambda P \sin\gamma \pm \sqrt{\frac{25}{144}\Lambda^2 P^2 (\sin\gamma)^2 + 1 + 2P^2 \sin 2\gamma} \qquad (3.16)$$

and solving the second equation in (3.15) for σ, we get:

$$\sigma = -\frac{4}{3}P^2 - \alpha a^2 - 2P^2 \cos 2\gamma - \frac{5}{2}\Lambda P a \cos\gamma \qquad (3.17)$$

The procedure followed to get the responses plotted in Figs. 3.3 and 3.4 is discussed here. We first choose Λ, P, and α; then we vary the value of γ from zero to 2π and for each γ, if the sum under the square root is real, we compute the values of 'a' from equation (3.16). Then, for each positive value of 'a', we compute the value of the detuning parameter, σ, from equation (3.17). Once we have the response amplitude, a, and the corresponding σ value, we take each of these pairs and plot them on the graph of a vs. σ.

Looking at Figs. 3.3 and 3.4, we notice that as the load amplitude, P, gets larger, the response amplitude gets larger. The only change occurring from Fig. 3.3 to Fig. 3.4 is that the stiffness value, α, is varied from -1 to 1. As we discuss the stability of these solutions, it is obvious that when P is small, as in Figs. 3.3a and 3.4a, we either have the trivial solution, which is unstable, or we have two nontrivial solutions besides the trivial one; only one of these three solutions is stable. As the value of the load amplitude, P, is increased, the number of solutions increases and so does the range of stability. We have to remember that between these two figures the only parameter changing is α; therefore the ranges of the detuning parameter σ for which solutions exist are different.

Checking Figs. 3.3b and 3.4b, we see that for σ sufficiently small or large, we do not have any solutions besides the trivial one, which is unstable. As we move from the left side of the graph to the right side, the number of solutions changes from one to three,

then to five, then back to three, and finally back to one. Now we consider Figs. 3.3c and 3.4c. The trivial solution is also unstable in this case. Looking at the graph at different points, we see that there are up to four nontrivial solutions at a time for some parts of the graph. As before, from these four nontrivial solutions, only two are stable. When we only have two nontrivial solutions, only one is stable.

In the last graphs of Figs. 3.3 and 3.4, we have two bifurcation points. Only between these two points is the trivial solution ($a = 0$) stable. The solutions are much more spread out and the response amplitude is much higher. We also find at different points of the graph that there exists more than one solution at a time and two of these are stable. Again, it is noticeable on the figures that the stability of the nontrivial solutions only changes at a vertical tangent or at $a = \frac{1}{\sqrt{2}}$ (see Fig. 3.3c), while in the case of the trivial solution the change occurs at the bifurcation points.

Fig. 3.5 shows the response amplitude, a, versus the load amplitude, P. We only study the case of linear stiffness, ($\alpha = 0$). We notice that for $\sigma \neq 0$, the nontrivial solutions only exist if P is large enough. We also see that the vertical tangents where these nontrivial stable solutions begin to exist move farther to the right of the graph as $|\sigma|$ gets larger. When we vary the value of the detuning parameter, σ, we notice from the figure and the previous cases that the detuning parameter plays an important role in controlling the response of the self-excited system under parametric excitation.

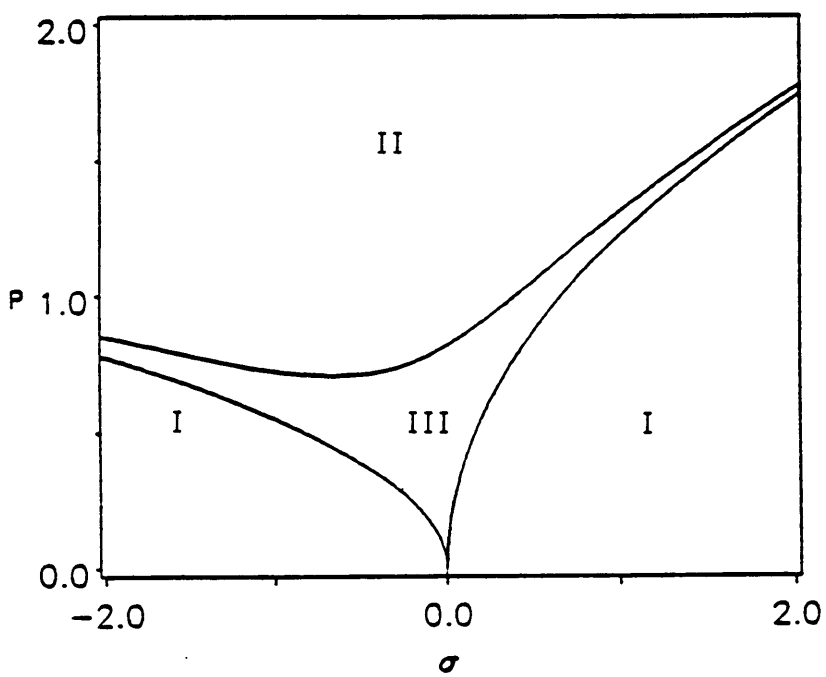

Figure 3.1. Regions of Existing Solutions, P vs. σ

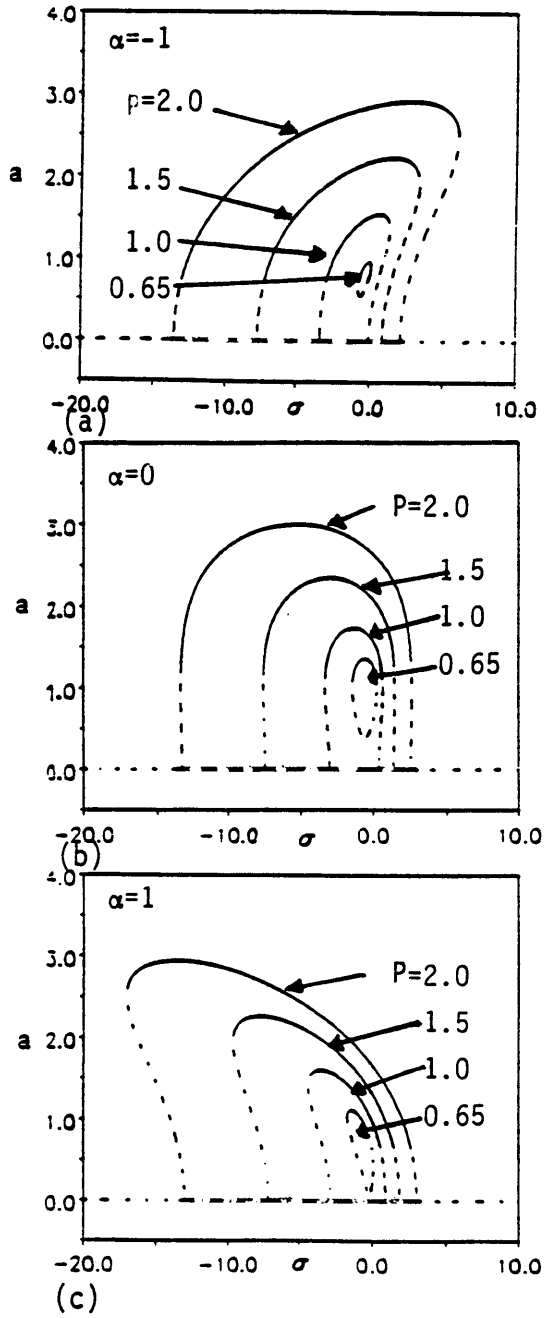

Figure 3.2. Frequency-Response Curves, a vs. σ

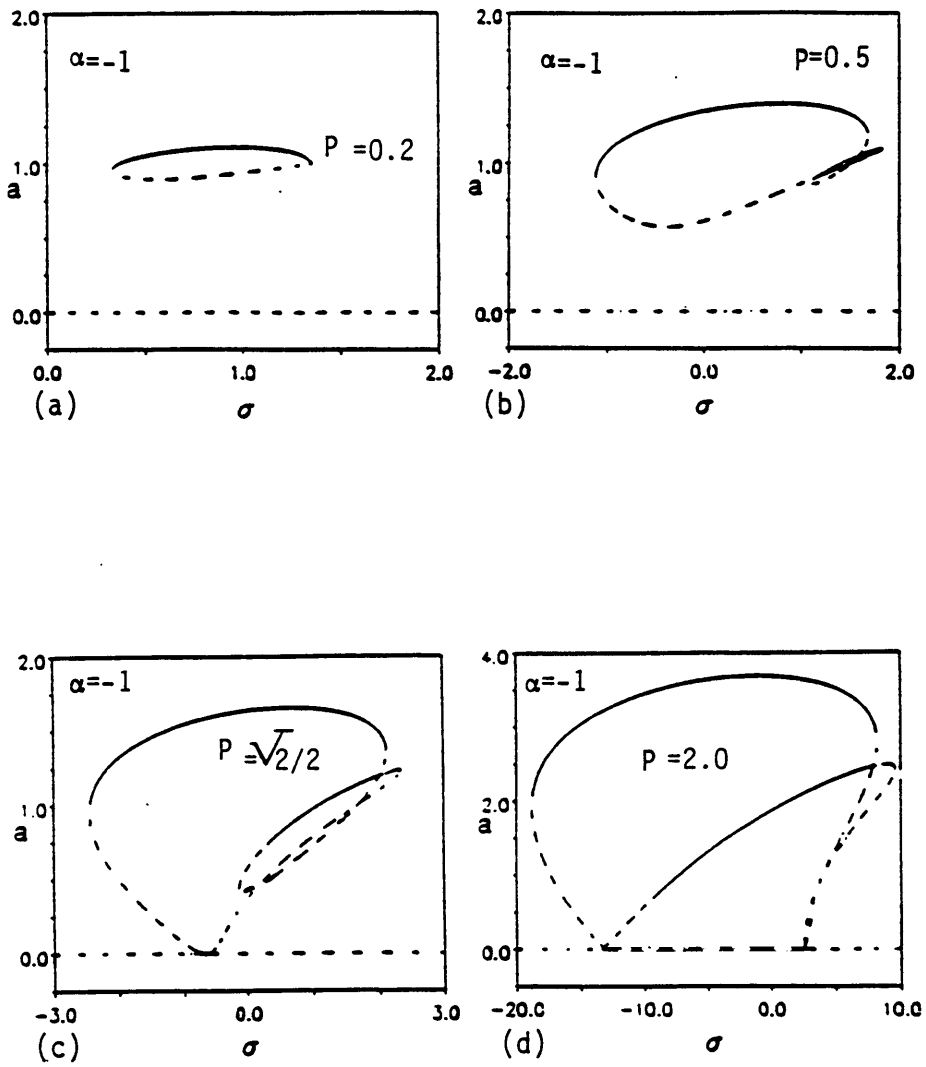

Figure 3.3. Frequency-Response Curves, a vs. σ

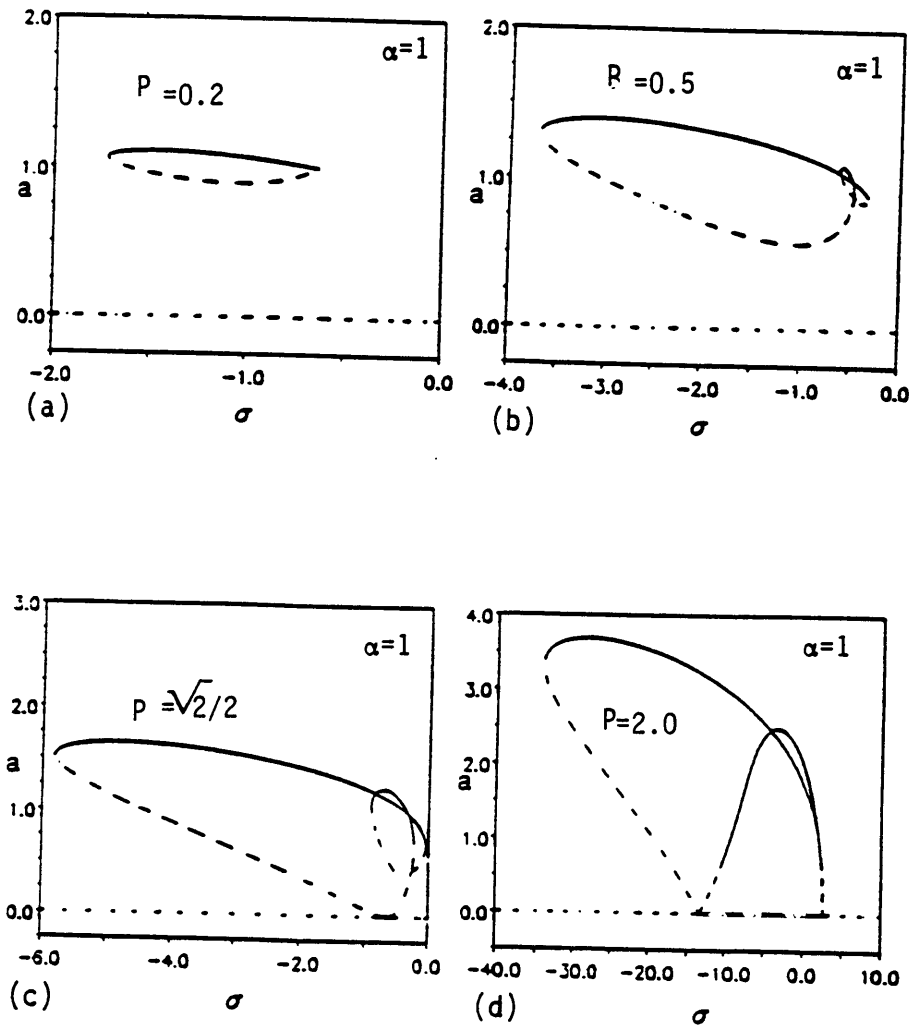

Figure 3.4. Frequency-Response Curves, a vs. σ

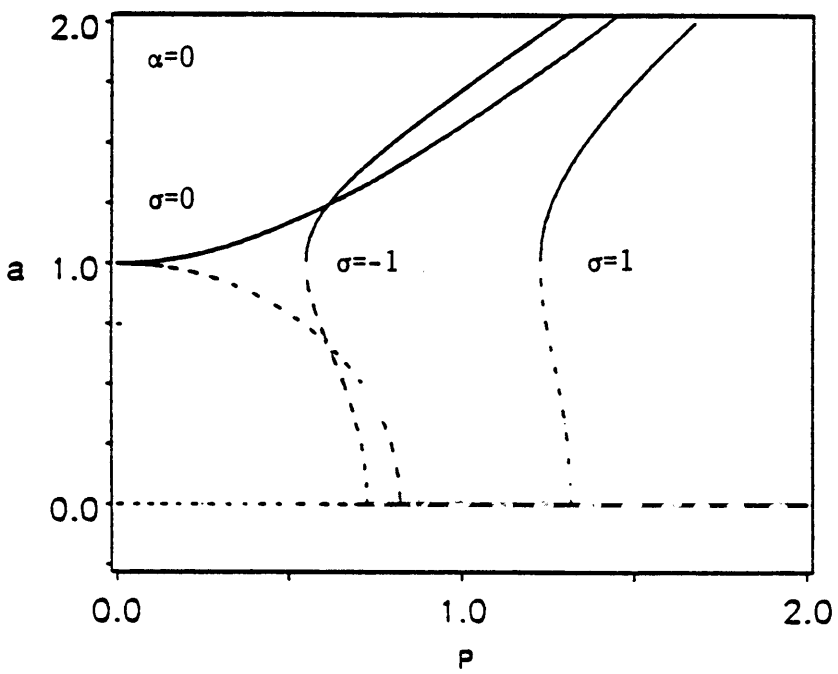

Figure 3.5. The Amplitude of The Response Versus The Load Amplitude

CHAPTER 4

CASE THREE : $\lambda_2 \pm \lambda_1 \simeq 2\omega$

In this particular chapter we discuss self-excited systems, under two different frequencies of parametric excitation, λ_1 and λ_2. These two parametric frequencies, λ_1 and λ_2, are assumed to satisfy the condition that their sum or difference is approximately equal to twice the natural frequency of the system, $\lambda_2 \pm \lambda_1 \simeq 2\omega$, or more accurately, $\lambda_2 \pm \lambda_1 = 2\omega + \varepsilon^2\sigma$, where

λ_1 is the frequency of the first parametric excitation,

λ_2 is the frequency of the second parametric excitation,

ε is a small parameter,

σ is the detuning parameter.

Of course each one of the components of the excitation will have its corresponding load amplitude, P_m, and a phase, τ_m.

To the governing equation of motion presented in the introductory chapter, we add the second parametric excitation and equation (1.2) becomes:

$$\begin{aligned} &\ddot{u} + \omega^2 u + \varepsilon\Lambda u^2 + \varepsilon^2\Gamma u^3 - 2\varepsilon^2 B\dot{u} + \varepsilon^2 C u^2 \dot{u} \\ &+ \varepsilon^2 D\dot{u}^3 + 2\varepsilon \sum_{m=1}^{2} \cos(\lambda_m t + \tau_m) Q^m(\varepsilon) u = 0 \end{aligned} \tag{4.1}$$

where

$$Q^m(\varepsilon) = 2\omega P_m, \qquad m = 1,2$$

Expanding equation (4.1), we get:

$$\begin{aligned} &\ddot{u} + \omega^2 u + \varepsilon\Lambda u^2 + \varepsilon^2\Gamma u^3 - 2\varepsilon^2 B\dot{u} \\ &+ \varepsilon^2 C u^2 \dot{u} + \varepsilon^2 D\dot{u}^3 + 4\varepsilon\omega u[P_1 \cos(\lambda_1 t + \tau_1) + P_2 \cos(\lambda_2 t + \tau_2)] = 0 \end{aligned} \tag{4.2}$$

The method of multiple scales [4] was again used here to solve the nonlinear equation. We will begin the study by checking the linear case, $\alpha = 0$ ($\Lambda = 0, \Gamma = 0$). As we get to the solution, some new variables are introduced:

$$e = -2\omega\{(R_1 + S_1)P_1^2 + (R_2 + S_2)P_2^2\} \tag{4.3}$$

and

$$h = -2\omega(S_1 + S_2)P_1P_2 \tag{4.4}$$

where

$$R_1 = -\frac{1}{\lambda_1(\lambda_1 + 2\omega)}$$

$$R_2 = -\frac{1}{\lambda_2(\lambda_2 + 2\omega)}$$

$$S_1 = -\frac{1}{\lambda_1(\lambda_1 - 2\omega)}$$

and

$$S_2 = -\frac{1}{\lambda_2(\lambda_2 - 2\omega)}$$

Only steady-state solutions are of interest. We have, as usual, a trivial solution, $a = 0$, and the nontrivial solutions are presented in the form of:

$$a^2 = \frac{1}{\xi}\{B \pm \sqrt{h^2 - (\frac{\sigma}{2} - e)^2}\} \tag{4.5}$$

We assume $\xi > 0$ and $B > 0$.

Solving the nonlinear stiffness case, $\alpha \neq 0$, for the nontrivial solutions, we get:

$$a^2 = \frac{2B\xi - (\sigma - 2e)\alpha \pm 2\sqrt{h^2\alpha^2 - B^2\alpha^2 + h^2\xi^2 - (\frac{\sigma}{2} - e)^2\xi^2 - B\xi\sigma\alpha}}{2(\xi^2 + \alpha^2)} \tag{4.6}$$

The same procedure explained in chapter 2 and discussed by Nayfeh and Mook [4] is used for checking the stability of the $\lambda_2 \pm \lambda_1 \simeq 2\omega$ case. Again the dashed lines imply instability of the response, and the solid lines imply stability of the response.

First we consider the case $P_1 = P_2 \equiv P$. For us to check the regions where solutions exist, we need to generate plots representing the load amplitude versus the detuning parameter, P *vs.* σ. Going back to equations (4.5) and (4.6) we set $a^2 = 0$ and solve the equations for σ. From (4.5) we get:

$$\sigma = -4\omega(R_1 + R_2 + S_1 + S_2)P^2 \pm 2\sqrt{4\omega^2(S_1 + S_2)^2P^4 - B^2} \tag{4.7a}$$

At vertical tangents on the plots of a vs. σ, we have:

$$\begin{cases} \sigma = -4\omega(R_1 + R_2)P^2 \\ \sigma = -4\omega(R_1 + R_2 + 2S_1 + 2S_2)P^2 \end{cases} \tag{4.7b}$$

From equation (4.6), for the nonlinear stiffness case, we get another system of two equations:

$$\begin{cases} \sigma = \dfrac{2}{\xi}\left[e\xi - B\alpha \pm \sqrt{h^2(\alpha^2 + \xi^2) - 2B\alpha e\xi}\,\right] \\ \sigma = 2\left[e \pm \sqrt{h^2 - B^2 - \dfrac{2B\xi e\alpha}{\alpha^2 + \xi^2}}\,\right] \end{cases} \tag{4.8}$$

All through the study of this case of $\lambda_2 \pm \lambda_1 \simeq 2\omega$, we work with two sets of λ_1 and λ_2 that satisfy the condition discussed at the beginning of this chapter:

$$\begin{cases} \lambda_1 = 0.5 \text{ and } \lambda_2 = 1.5 \\ \\ \lambda_1 = 0.5 \text{ and } \lambda_2 = 2.5 \end{cases} \tag{4.9}$$

As we look at Figs. 4.1 and 4.2 referring to the two different sets of λ_1 and λ_2, these figures represent in what ranges of P's and σ's solutions exist. As before, there is a region marked by I, and that is where there is only one solution, the trivial solution. Region III, right between regions I and II, is where three solutions exist, two of which are non-trivial solutions. Then we have region II, which shows the existence of only one non-trivial solution besides the trivial one. When the system stiffness is not equal to zero ($\alpha \neq 0$), we see that the system reacts by having different ranges of existing solutions. It is obvious on the graphs how the shapes of the regions vary as α is varied from -1 to 0, and then to 1.

Checking the response amplitude versus the detuning parameter (a vs. σ plots), we move to the two different sets of λ_1 and λ_2 satisfying the resonance condition (see eq. 4.9). In generating these graphs, we set a P value at each time and check the system response using eq. 4.5 or 4.6. It is expected that as we increase the magnitude of P we will get larger response amplitudes, and that is exactly what Figs. 4.3 and 4.4 show. Now, as we look at each graph in these two figures we see that the variable that is changing is the stiffness α. We see a slight decrease in the response magnitude in Fig. 4.3 when $\alpha \neq 0$. As for the stability, it is clear that as the responses get more spread out with larger load amplitudes, we get a larger region where the solutions are stable. Again stability is marked by solid lines and instability by dashed lines. We notice that stable nontrivial solutions start at the vertical tangents or at $a = \frac{1}{\sqrt{2}}$, ~~while the trivial solution is only stable between the bifurcation points~~.

Now we allow P_1 and P_2 to be different from each other. Figures 4.5 and 4.6 show the response amplitude versus one of the load amplitudes, a vs. P_1. In this case, we set

$$P_2 = 1\,, \quad \xi = 1, \quad \omega = 1, \quad \text{and } B = 1$$

and we vary the detuning parameter, σ, for each set of λ_1 and λ_2 (eq. 4.9). In Fig. 4.5, with $\lambda_1 = 0.5$ and $\lambda_2 = 1.5$ and linear stiffness, $\alpha = 0$, the response amplitude is high for negative values of the detuning parameter ($\sigma < 0$), and as we go towards large positive values of the detuning parameter ($\sigma > 0$), the response decreases and even disappears. The disappearance of the response at $\sigma > 0$ is also true for $\alpha \neq 0$, even though the response amplitude seems to be a lot higher for $\alpha < 0$ ($\alpha = -1$) and a lot smaller when $\alpha > 0$ ($\alpha = 1$). This figure leads us to notice once more the significant effect of the detuning parameter which when acting on a system can make it almost unresponsive to any disturbances.

Looking at Fig. 4.6, it is obvious that even though $\lambda_1 = 0.5$ and $\lambda_2 = 2.5$, the system is responding the same way as in the case plotted in Fig. 4.5. The only noticeable difference is in the shape of the response, meaning the range of σ's at which we have solutions. Other than that, when $\sigma < 0$, the response is high and it starts disappearing as we get to larger positive values of the detuning parameter. Also, the same remark can be mentioned about the response magnitudes being a little higher for $\alpha = -1$ and a little lower for $\alpha = 1$ in comparison with the linear stiffness case, $\alpha = 0$.

As for the stability of the solutions plotted in these two figures (4.5 & 4.6), we see that when the detuning parameter is negative, $\sigma < 0$, or closer to zero, for a perfectly tuned system, we have a larger number of stable solutions. It is expected since the response dies out for values of σ larger than zero. Again, instability of the trivial solution corresponding to each response curve is only marked up to the first bifurcation point

coming from the right and the first bifurcation point coming from the left. This is due to the fact that we have more than one response plotted in each graph. Therefore, what is needed to remember is that the trivial solution is only stable between the bifurcation points, while the nontrivial solutions start being stable at the vertical tangents or at $a = \frac{1}{\sqrt{2}}$.

Figures 4.7 and 4.8 also show the response amplitude versus one of the load amplitudes, a vs. P_1, however this time $P_2 = P_1 \equiv P$. Therefore, as we vary P_1 in our study we are also varying P_2. Another difference is that we are only checking a small range of the detuning parameter; σ is first set equal to unity, then to zero, for a perfectly tuned system, then again to negative one. We notice immediately in these two figures that when the system is perfectly tuned and has a linear stiffness, $\alpha = 0$, it does not take much load at all for the system to reach a response. For $\sigma \neq 0$, the load at which the response becomes stable is much higher; this is also true for $\sigma = 0$ when the stiffness is nonlinear, $\alpha \neq 0$. In Fig. 4.7, we see that as we move from the graph representing $\alpha = -1$ to the one representing $\alpha = 1$, the response amplitude starts high for low values of P_1 and as we get to $\alpha = 1$ it takes much more load for much less response. Another significant point: the bifurcation load when $\alpha = -1$ is larger than in the other cases; also, for $\sigma = 1$ it seems that the bifurcation load is the largest in all the cases. When $\lambda_1 = 0.5$ and $\lambda_2 = 2.5$, or taking a look at Fig. 4.8, we see the same facts discussed in Fig. 4.7. For an increasing load amplitude P we get an increasing response, which is slightly altered or decreased when we have a nonlinear stiffness. The difference is that it seems that in this case the bifurcation load is the largest when $\sigma = -1$. Also we notice that the loads at which each nontrivial solution begins to be stable are slightly altered. In these two figures, as expected, the range of unstable solutions decreases as both the system stiffness and the detuning parameter are equal to zero.

Now we get to Figs. 4.9, 4.10, and 4.11. In generating these plots we are dealing with the case:

$$\lambda_1 + \lambda_2 = 2\omega \ .$$

We let:

$$\Gamma = \frac{\lambda_1}{2\omega}$$

and

$$\xi = 1 \ , \ \ B = 1, \ \ P_1 = P_2 = 1, \ \omega = 1$$

For each plot we set a detuning parameter, σ, to a value and check the response amplitude by varying Γ along the x-axis between zero and one ($0 < \Gamma < 1$). We compute all the parameters, R_1, R_2, S_1, S_2 , e, and h, needed to compute the response amplitudes, a, which are then plotted in Figs. 4.9, 4.10, and 4.11. The only changing variable in these three different sets of plots is the stiffness of the system, α(-1,0,1). Before we go any further in discussing these three figures, we should notice that the solutions obtained near $\gamma = 0, 0.5$, and 1 are not valid due to the existence of other resonances.

When the stiffness is negative, or $\alpha = -1$, as we vary σ from a high positive value to a value closer to zero, we see in Fig. 4.9a that there is a very small range of Γ's at which we get a stable nontrivial solution. The trivial solution is only stable when there is one nontrivial solution. In Fig. 4.9b, the stable nontrivial response is spread out more, and an unstable nontrivial solution is building up. In these figures we find up to three solutions at a time, two of which are nontrivial and only one of these is stable. The nontrivial solution that is building up in Fig. 4.9b, splits up from the stable part in Fig. 4.9c, and forms a small unstable solution at low response amplitudes. At the same time the stable nontrivial solution takes over and at any Γ on the x-axis we have a stable nontrivial solution and an unstable trivial one. In Fig. 4.9d, when the system is perfectly

tuned, the nontrivial unstable independent solution disappears and we are left with just one nontrivial solution that is stable everywhere on the interval.

Looking at Fig. 4.10, we follow a nice build-up of the response as the detuning parameter, σ, is varied in a linear stiffness system, $\alpha = 0$. Starting with large negative values of σ, then moving towards a perfectly tuned system ($\sigma = 0$), then again applying large positive values of the detuning parameter, we see how at first nontrivial solutions only exist at values of Γ close to zero and close to unity. In these two small areas of existing response we have three solutions, an unstable trivial, an unstable nontrivial, and a stable nontrivial one. As the detuning parameter is varied to a value equal to zero, the stable nontrivial solution is spreading out more and more along the interval of Γ . The nontrivial unstable solution disappears completely at $\sigma = 0$, just like in the $\alpha = -1$ case. When we start varying σ again to larger positive values, the small nontrivial unstable solution reappears, then connects with the stable part, then at the end we have the same response behavior as we started with in Fig. 4.10a.

When the stiffness parameter is positive, $\alpha = 1$, solutions exist as we vary the detuning parameter, σ, from large negative values to zero, a perfectly tuned system. In Fig. 4.11, we show the development of the response as σ is varied. Again we see the same trend: three solutions exist at Γ's about zero and unity, and only one is stable at a time. As we go on towards $\sigma = 0$, the nontrivial unstable solution splits up and gets smaller until it disappears. Meanwhile, the stable nontrivial solution is spreading out more, and at any point between zero and one we have a stable nontrivial solution and a trivial solution unstable everywhere.

Concluding the discussion about these three figures, 4.9, 4.10, and 4.11, an important fact to remember is that only when the stiffness is linear does the system pick up and

respond again as we go beyond $\sigma = 0$ in absolute value. For the nonlinear stiffness, the response stagnates at $\sigma = 0$ no matter how large we make the detuning parameter. There may be an explanation to this: it seems that we have forgotten all about the response when the stiffness is varied from -1 to 0, and then to 1. Let's take a close look at different detuning parameter values at which solutions exist, when $\alpha = -1$ (Fig. 4.9), $\alpha = 0$ (Fig. 4.10), and $\alpha = 1$ (Fig. 4.11). For $\alpha = -1$, we notice that solutions exist as we come down from high positive values of the detuning parameter and this number of solutions stagnates at $\sigma = 0$, which in comparison with all the previous cases we studied, is synonymous with the motion of the response to the right, and the opposite for $\alpha = -1$ is true. When $\alpha = 0$ the response is usually symmetric about the $\sigma = 0$ value, which is also true for this case and well shown in Fig.4.10.

Finally, we get to the last discussion of this chapter, and Figs. 4.12, 4.13, and 4.14. Again, Fig. 4.12 deals with the stiffness equal to negative one, Fig. 4.13, when the stiffness is linear, and in Fig. 4.14, the stiffness is equal to positive one. Let's start by explaining the different parameters and the way these figures have been generated. First, we are imposing a condition on the λ's :

$$\lambda_2 - \lambda_1 = 2\omega$$

We let

$$\gamma = \frac{\lambda_1}{\lambda_2}$$

We vary γ along the x-axis between zero and unity, and we assume:

$$\xi = 1\ , \quad B = 1, \quad P_2 = P_1 = 1, \quad \text{and } \omega = 1.$$

Again we compute all the needed parameters (R's, S's, e and h), to be able to compute the response amplitude, a, and plot it. In generating the different graphs belonging to each figure, we are only varying the detuning parameter, σ, and examining the effect on the system. In this case we also have a similar type of behavior as seen in Figs.4.9, 4.10,

and 4.11, the solutions near $\gamma = 0$, $\frac{1}{3}$, and 0.5 are not valid due to the existence of other resonances in the system.

Looking at Fig. 4.12, we notice that at any value of the detuning parameter, σ, we have an asymptote at $\gamma = 0.5$, where the second parametric frequency is twice the first. We change the detuning parameter value, σ, from high negative values to high positive values, and we look at the development of the different solutions. At first, when $\sigma < 0$, we have an unstable trivial solution and a very small response builds up for γ close to 0.5. Then the stable response abruptly approaches an infinite amplitude at $\gamma = 0.5$. For $\sigma = 0$, or a perfectly tuned system, the same behavior takes place, but this time there is a smoother movement towards the infinite amplitude. There is also a small nontrivial unstable solution that appears at $\gamma \simeq 0.5$. It grows larger as we increase the detuning parameter, then slowly connects to the stable nontrivial solution. At the same time, a small portion of the nontrivial unstable solution breaks free and becomes an independent solution on the left of the graph, which disappears as the detuning parameter gets larger ($\sigma \simeq 220$). As for the stable solution near $\gamma = 0.5$, the response does not appear to be affected much by increasing the detuning parameter; the curve just flattens out slowly and will eventually look like a vertical straight line.

Moving along to Fig. 4.13, or the linear stiffness case, we see a lot of similarities in the behavior as in Fig. 4.12: first, the development of an independent response that connects to the stable nontrivial solution; second, the breaking free of a portion of the nontrivial solution and its disappearance at high magnitudes of the detuning parameter; also, the large stable solution that suddenly appears at $\gamma = 0.5$, and so on. The one obvious difference is the fact that in this case, the end response shifts and faces the right

side to the contrary of the case $\alpha = -1$, but then again this is where the change in the system stiffness plays a role.

As we get to the last figure in the set, and in the chapter, Fig. 4.14, where the stiffness is positive and equal to unity, we notice that the response is similar to the other two cases but for the sequence it follows. There is no independent solution appearing or disappearing from the graphs, and the nontrivial solution stays together at all times with no breaks in it. We have a trivial unstable solution and a nontrivial stable solution; the only active part is the nontrivial unstable solution. It gets larger, then it decreases, and then it almost disappears, by flattening out with a very small curve facing the right side. Again, we see the same trend of motion in the solutions as the stiffness value is varied, and the linear stiffness case here is not perfectly symmetric, but tries to have solutions belonging to both the case $\alpha = -1$ and the case $\alpha = 1$.

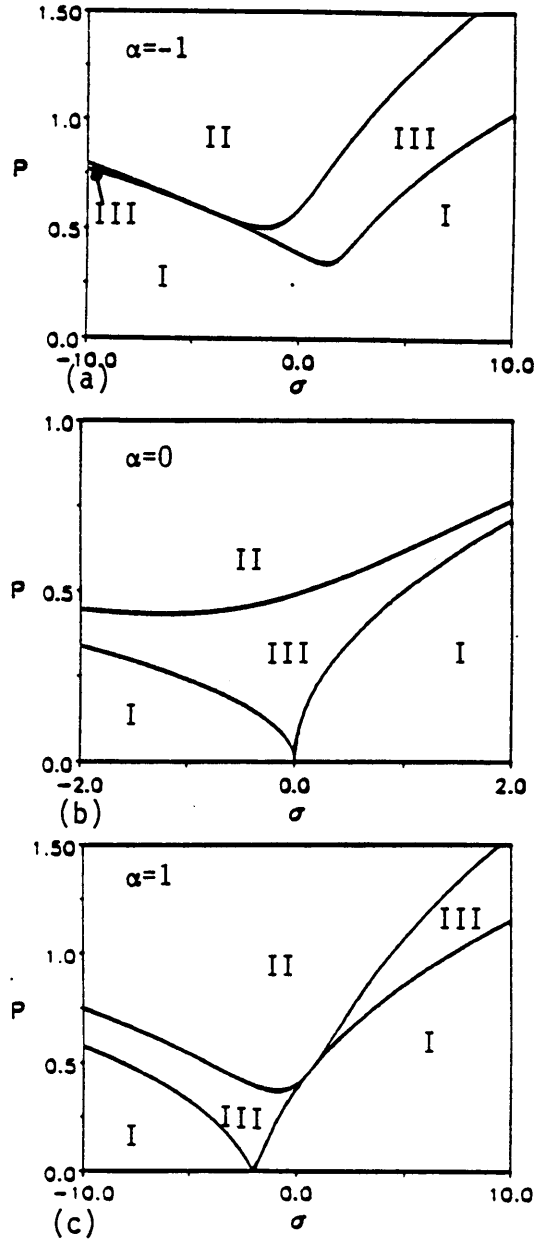

Figure 4.1. Regions of Existing Solutions, $\lambda_1 = 0.5$ and $\lambda_2 = 1.5$

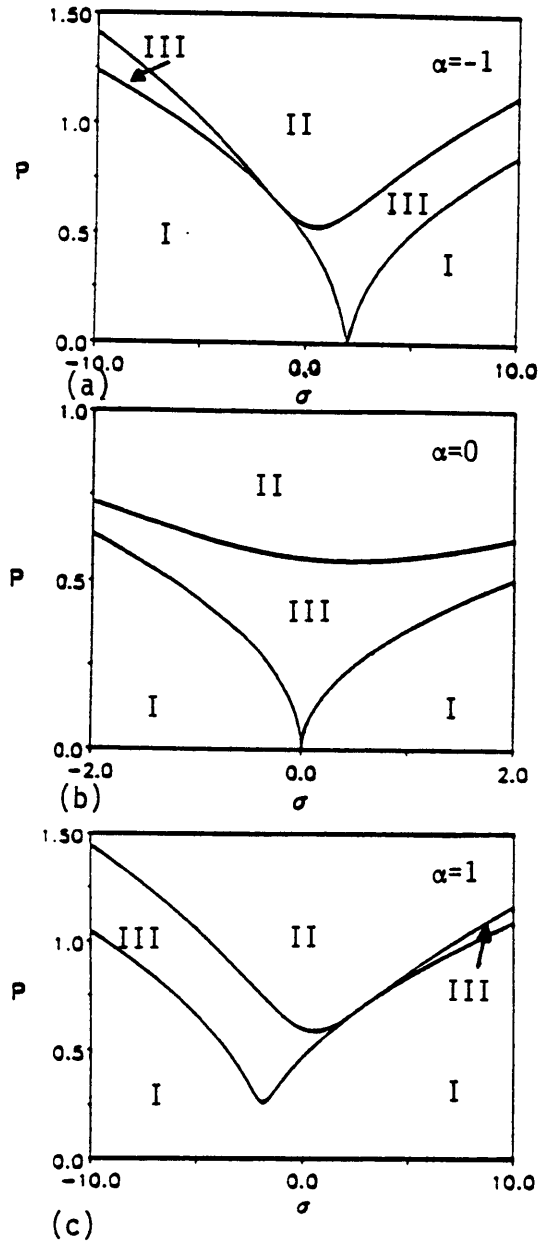

Figure 4.2. Regions of Existing Solutions, $\lambda_1 = 0.5$ and $\lambda_2 = 2.5$

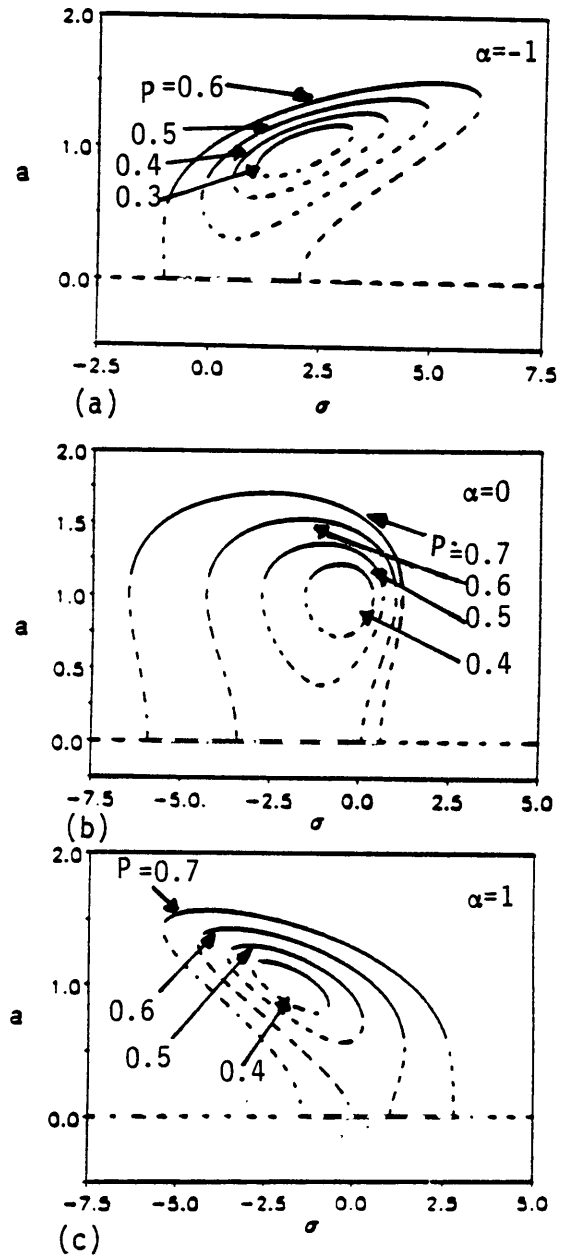

Figure 4.3. Frequency-Response Curves, a vs. σ, $\lambda_1 = 0.5$ and $\lambda_2 = 1.5$

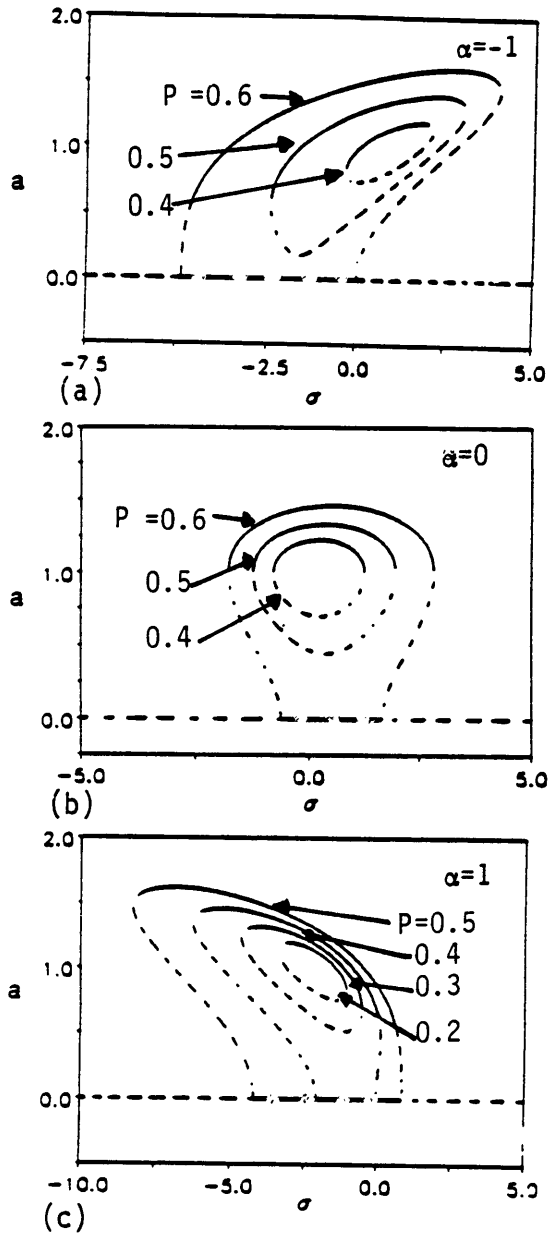

Figure 4.4. **Frequency-Response Curves,** a vs.σ, $\lambda_1 = 0.5$ and $\lambda_2 = 2.5$

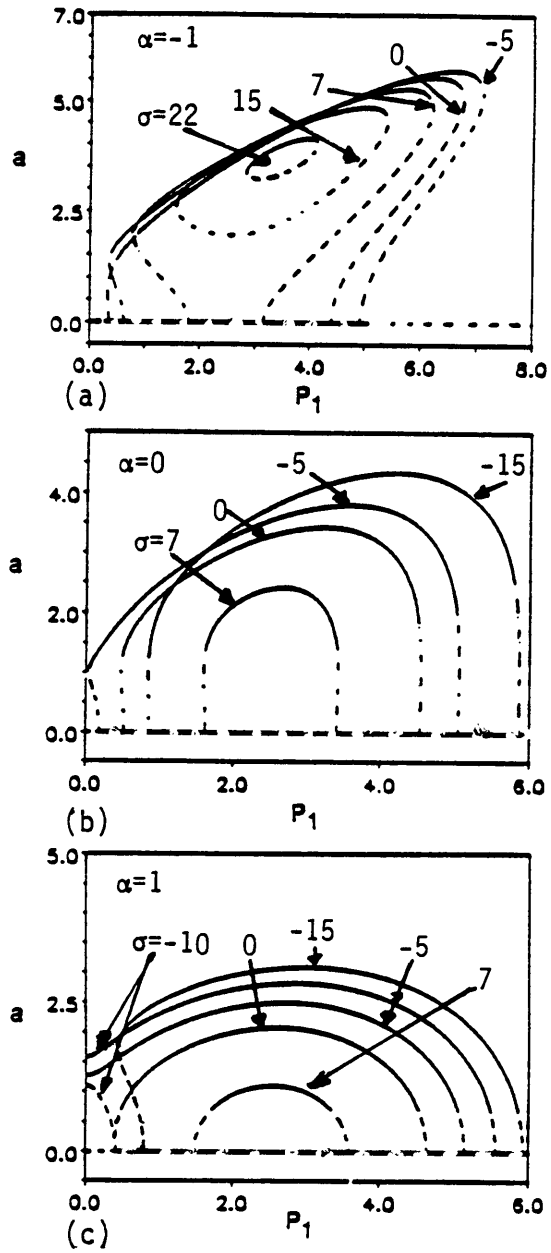

Figure 4.5. The Response Amplitude Versus One of The Load Amplitudes, a vs P_1, $\lambda_1 = 0.5$ and $\lambda_2 = 1.5$

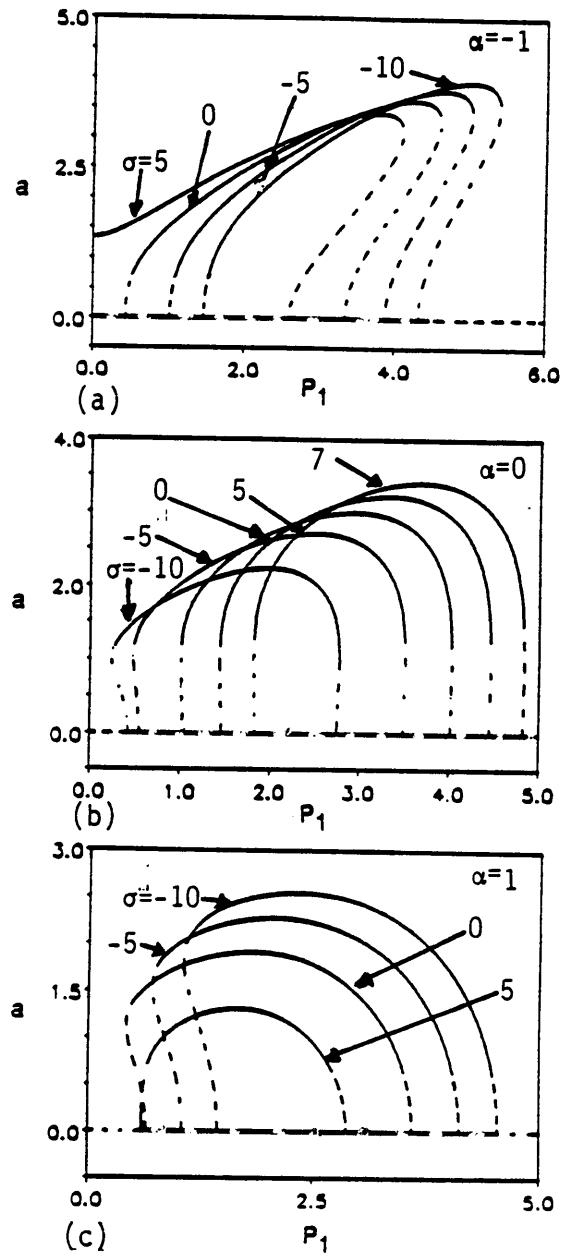

Figure 4.6. The Response Amplitude Versus One of The Load Amplitudes, a vs P_1, $\lambda_1 = 0.5$ and $\lambda_2 = 2.5$

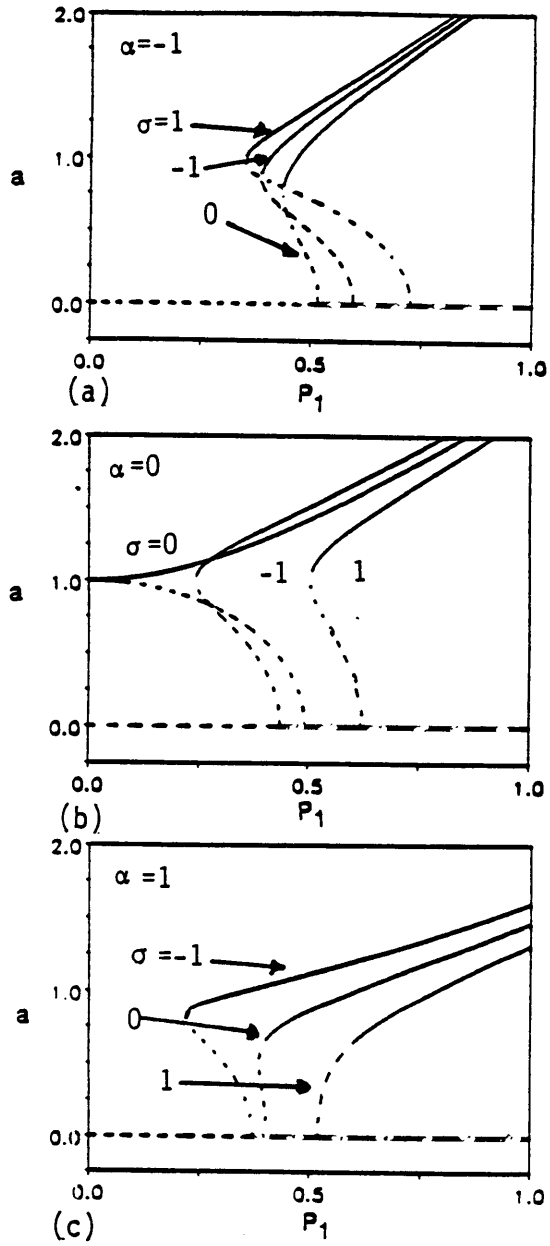

Figure 4.7. The Response Amplitude Versus The Load Amplitude When $P_1 = P_2 = P$ and $\lambda_1 = 0.5$ and $\lambda_2 = 1.5$

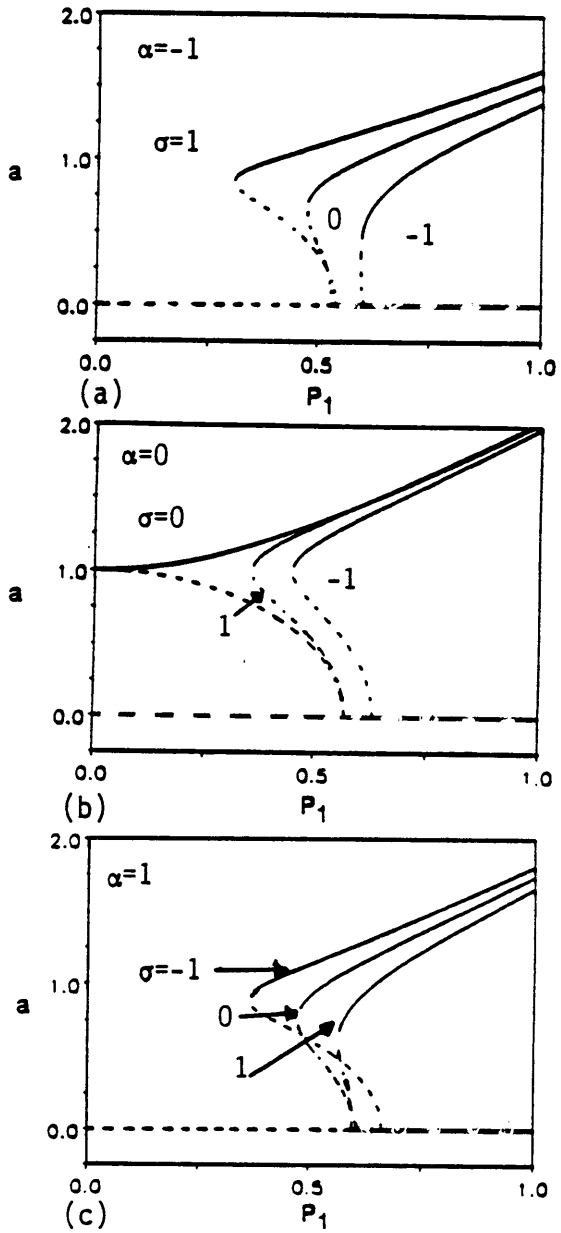

Figure 4.8. The Response Amplitude Versus The Load Amplitude When $P_1 = P_2 = P$ and $\lambda_1 = 0.5$ and $\lambda_2 = 2.5$

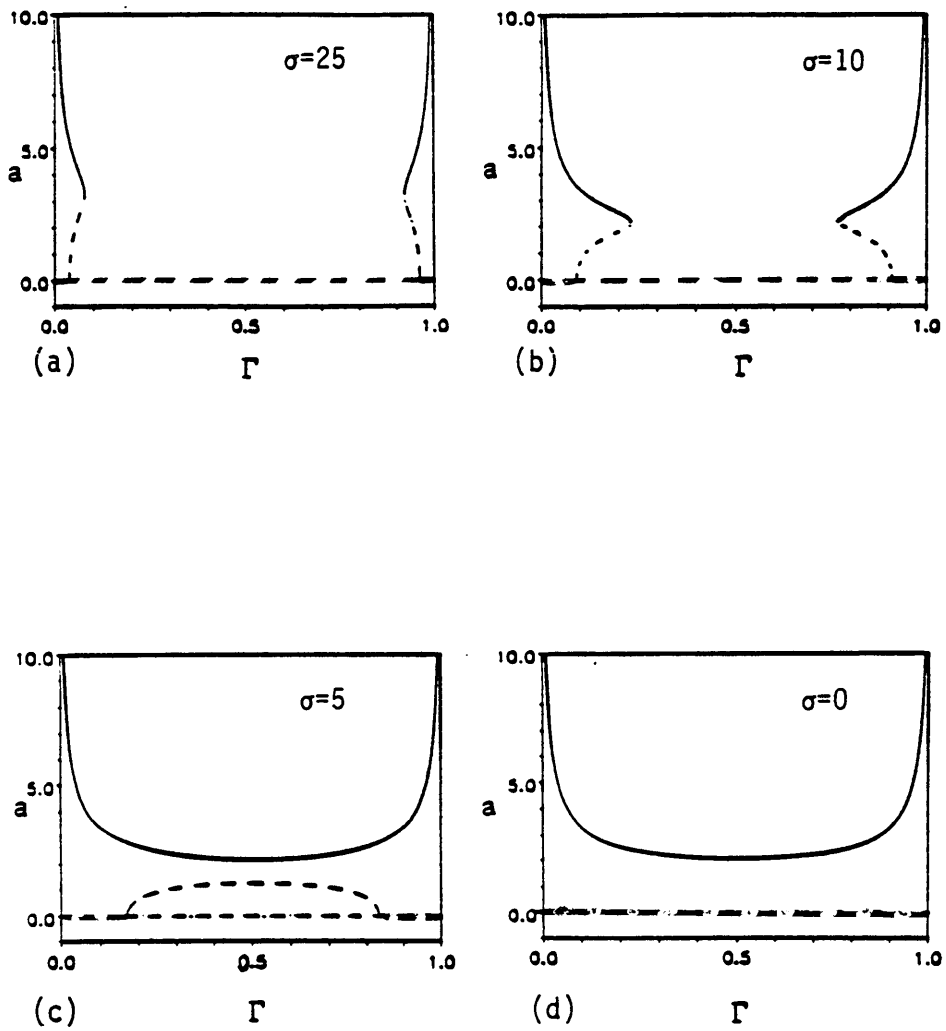

Figure 4.9. **The Response Amplitude Versus Relative Frequencies,** a **vs.** Γ , where $\Gamma = \frac{\lambda_1}{2\omega}$, $\lambda_1 + \lambda_2 = 2\omega$ and $\alpha = -1$

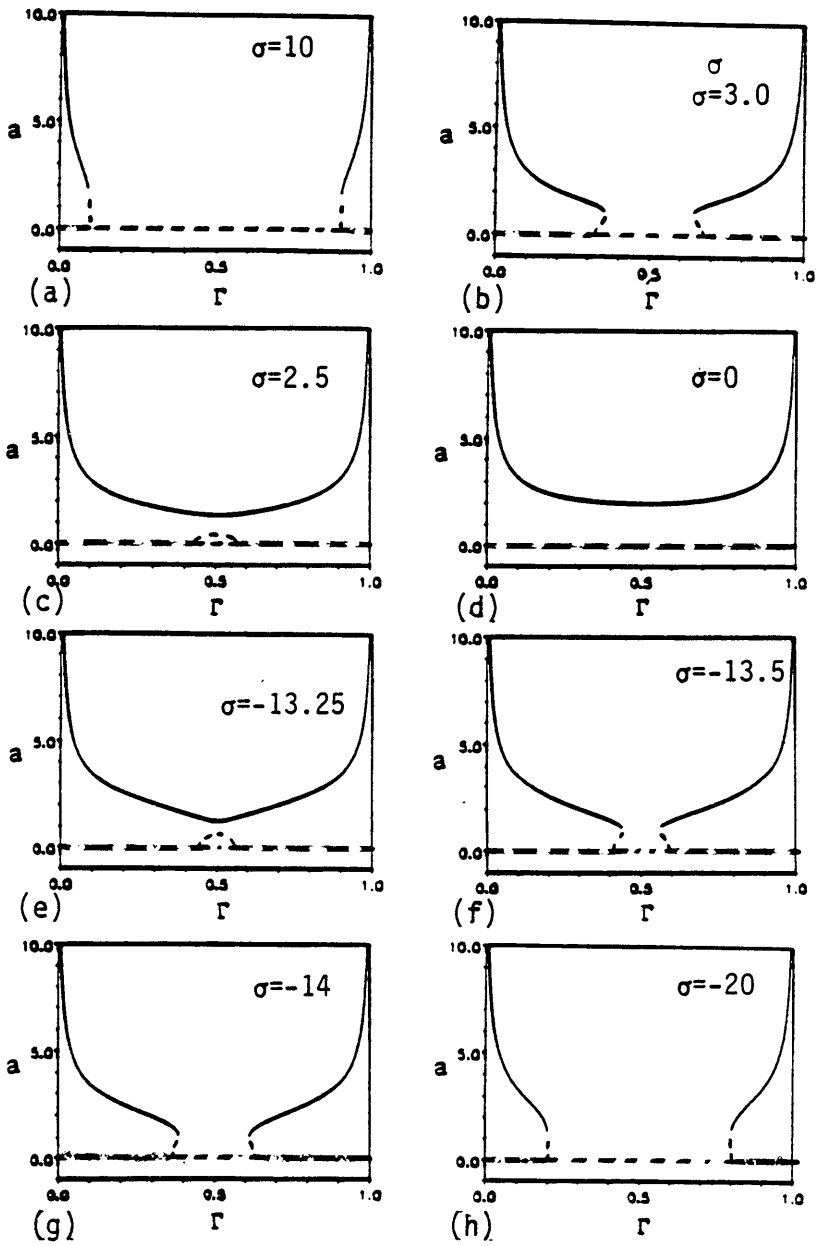

Figure 4.10. The Response Amplitude Versus Relative Frequencies, a vs. Γ , where $\Gamma = \frac{\lambda_1}{2\omega}$, $\lambda_1 + \lambda_2 = 2\omega$ and $\alpha = 0$

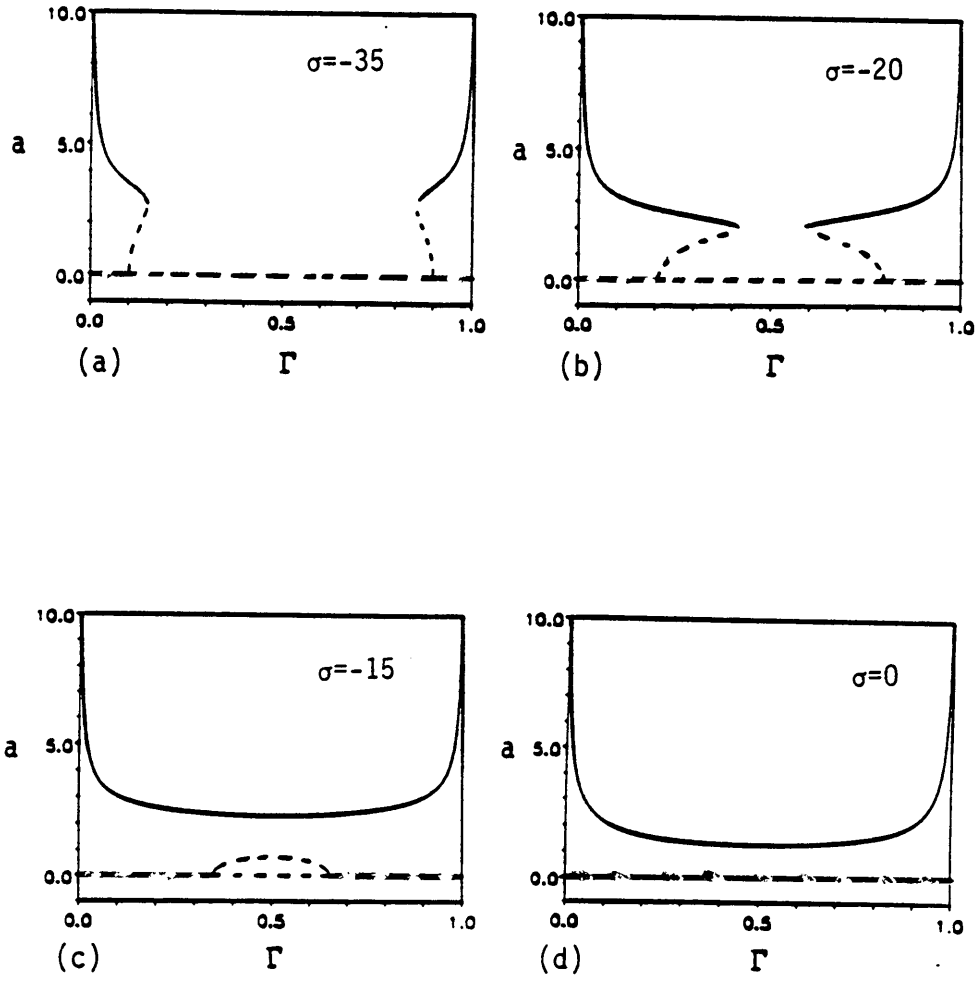

Figure 4.11. The Response Amplitude Versus Relative Frequencies, a vs. Γ , where $\Gamma = \frac{\lambda_1}{2\omega}$, $\lambda_1 + \lambda_2 = 2\omega$ and $\alpha = 1$

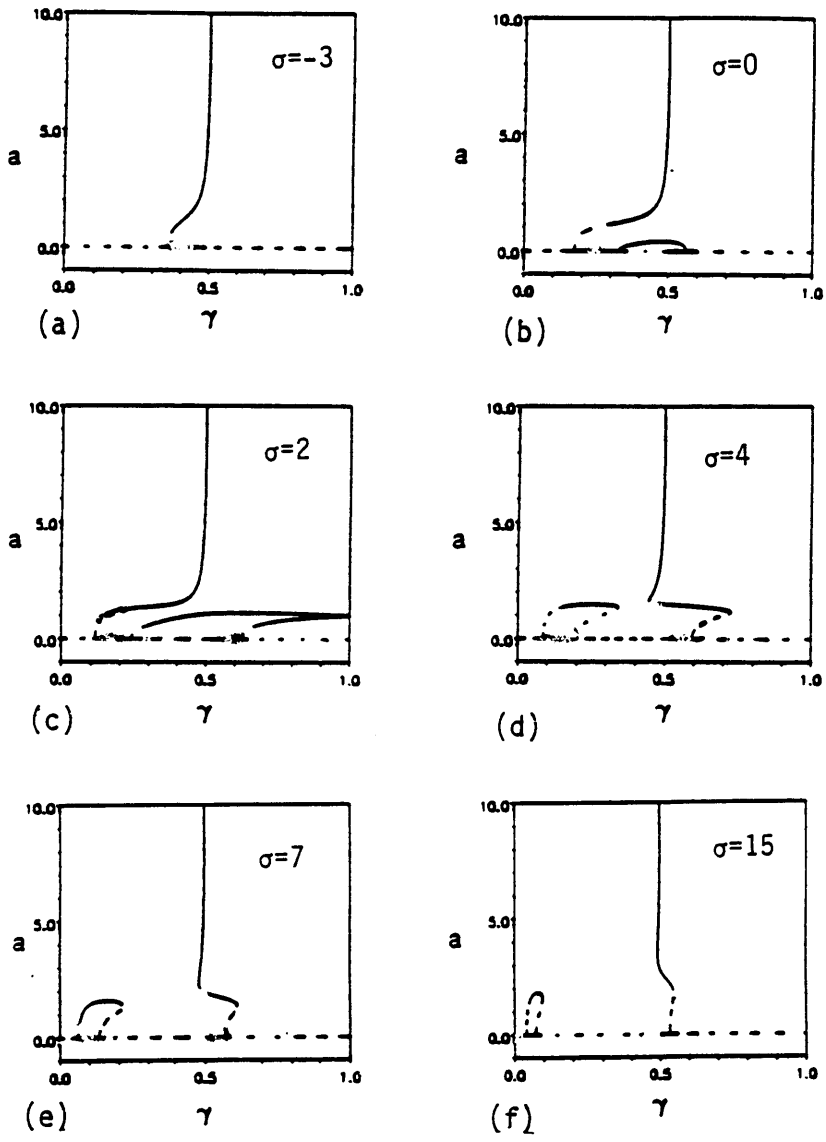

Figure 4.12. **The Response Amplitude Versus Relative Frequencies,** a **vs.** γ , where $\gamma = \frac{\lambda_1}{\lambda_2}$, $\lambda_2 - \lambda_1 = 2\omega$ and $\alpha = -1$

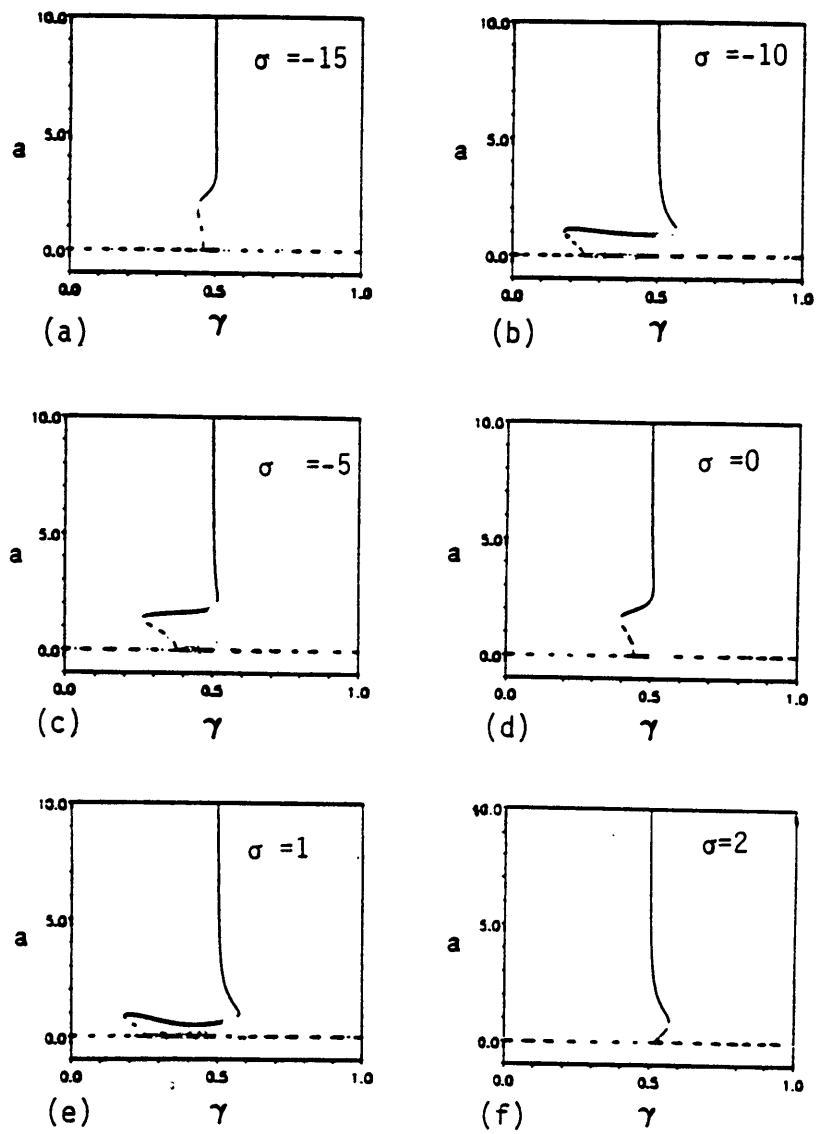

Figure 4.13. **The Response Amplitude Versus Relative Frequencies,** a **vs.** γ , where $\gamma = \frac{\lambda_1}{\lambda_2}$, $\lambda_2 - \lambda_1 = 2\omega$ and $\alpha = 0$

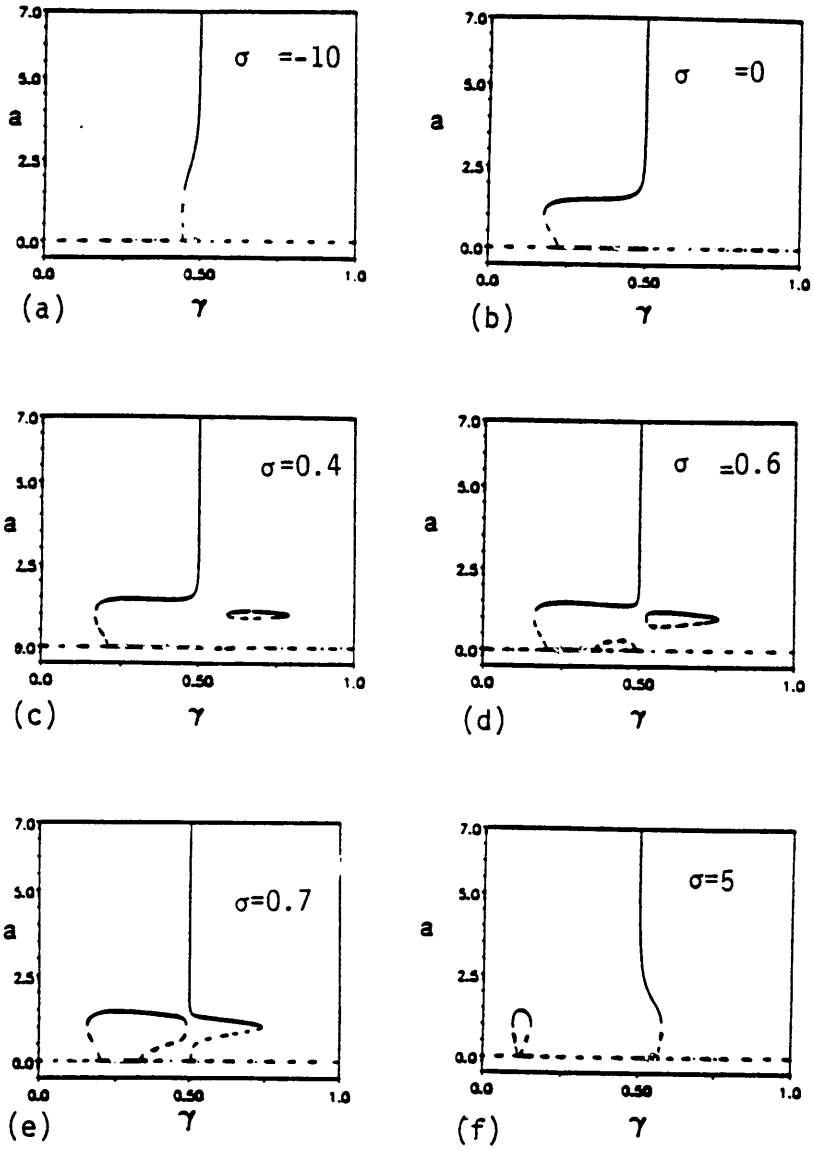

Figure 4.14. The Response Amplitude Versus Relative Frequencies, a vs. γ , where $\gamma = \frac{\lambda_1}{\lambda_2}$, $\lambda_2 - \lambda_1 = 2\omega$ and $\alpha = 1$

CHAPTER 5

CASE FOUR : $\lambda_1 + \lambda_2 \simeq \omega_r - \omega_q$

In this chapter, the case under study is when the resonance involves two natural frequencies, ω_r and ω_q, and two parametric excitation frequencies, λ_1 and λ_2. We are assuming that the sum of the two parametric frequencies is near the difference of the two natural frequencies with no other resonances existing. We let:

$$\lambda_1 + \lambda_2 = \omega_r - \omega_q + \varepsilon^2 \sigma$$

When the system stiffness is linear, which is the case in this chapter, the governing set of equations has the form:

$$\ddot{u}_n + \omega_n^2 u_n - 2\varepsilon^2 \sum_{j=r,q} B_{jn}\dot{u}_j + \varepsilon^2 \sum_{j=r,q}\sum_{k=r,q}\sum_{l=r,q}(C_{jkln}u_j u_k \dot{u}_l + D_{jkln}\dot{u}_j\dot{u}_k\dot{u}_l)$$
$$+ 4\varepsilon\omega_n \sum_{m=1}^{2} \cos(\lambda_m t + \tau_m) \sum_{j=r,q} P_{jn}^m u_j = 0, \qquad n = q,r \tag{5.1}$$

Expanding (5.1), and using the knowledge we acquired in chapter four about two parametric frequencies acting on the system, we will get a system of linear equations that we solve applying the method of multiple scales [4]. The solution comes out in the following form:

$$\begin{aligned} &- B_{qq}a_q + \xi_{qq}a_q^3 + \xi_{rq}a_q a_r^2 + g_{rq}a_r \sin\gamma = 0 \\ &- B_{rr}a_r + \xi_{qr}a_q^2 a^r + \xi_{rr}a_r^3 - p_{qr}a_q \sin\gamma = 0 \\ &(\sigma - e_r + e_q)a_q a_r = (g_{rq}a_r^2 - p_{qr}a_q^2)\cos\gamma \end{aligned} \tag{5.2}$$

where g_{rq}, p_{qr}, e_q, e_r, ξ_{qq}, ξ_{qr}, ξ_{rq}, and ξ_{rr} are defined in the appendix.

Examining the equations above, it is obvious that there is a trivial solution $a_q = a_r = 0$. To find the nontrivial solutions, we start by multiplying the first equation in (5.2) by $p_{qr}a_q$, and the second equation in (5.2) by $g_{rq}a_r$. The result is eq. 5.3a and eq. 5.3b, respectively:

$$- B_{qq}p_{qr}a_q^2 + \xi_{qq}p_{qr}a_q^4 + \xi_{rq}p_{qr}a_q^2 a_r^2 + g_{rq}p_{qr}a_q a_r \sin\gamma = 0 \tag{5.3a}$$

and

$$- B_{rr}g_{rq}a_r^2 + \xi_{qr}g_{rq}a_q^2a_r^2 + \xi_{rr}g_{rq}a_r^4 - g_{rq}p_{qr}a_qa_r \sin\gamma = 0 \qquad (5.3b)$$

We add (5.3a) to (5.3b), and we eliminate $\sin\gamma$, to get:

$$- B_{qq}p_{qr}a_q^2 - B_{rr}g_{rq}a_r^2 + \xi_{qq}p_{qr}a_q^4 + \xi_{rr}g_{rq}a_r^4 + (\xi_{rq}p_{qr} + \xi_{qr}g_{rq})a_q^2a_r^2 = 0 \qquad (5.4)$$

We let $X = a_q^2$ and $Y = a_r^2$, and obtain:

$$- B_{qq}p_{qr}X - B_{rr}g_{rq}Y + \xi_{qq}p_{qr}X^2 + \xi_{rr}g_{rq}Y^2 + (\xi_{rq}p_{qr} + \xi_{qr}g_{rq})XY = 0 \qquad (5.5)$$

which we can write as:

$$a_0X^2 + b_0X + c_0 \qquad (5.6)$$

where

$a_0 = \xi_{qq}p_{qr}$

$b_0 = - B_{qq}p_{qr} + (\xi_{rq}p_{qr} + \xi_{qr}g_{rq})Y$

$c_0 = - B_{rr}g_{rq}Y + \xi_{rr}g_{rq}Y^2$

In generating the response, we use the following parameters:

$B_{qq} = 1$, $B_{rr} = 2$

$\xi_{qq} = 1$, $\xi_{qr} = -1$, $\xi_{rq} = -1$, $\xi_{rr} = 2$

$\omega_q = 1$, $\omega_r = 2.3$

$\lambda_1 = 0.4$, $\lambda_2 = 0.9$

We also set $P^1_{qq} = P^1_{qr} = P^1_{rq} = P^1_{rr} = P^2_{qq} = P^2_{qr} = P^2_{rq} = P^2_{rr} \equiv P$. In the study the P value is varied. Then we compute the following parameters (check appendix for calculation procedure): g_{rq}, p_{qr} , e_q, and e_r.

Once all the preliminary calculations are done, we look back to eq. 5.6 and we vary the Y between zero and four ($0 < Y < 4$). We determine a_0, b_0, and c_0 for each Y and check if

$$b_0^2 - 4a_0c_0 < 0 \tag{5.7}$$

which means there is no solution. If eq. 5.7 is not satisfied, then we compute:

$$X_1 = \frac{1}{2a_0}(-b_0 + \sqrt{b_0^2 - 4a_0c_0})$$

and

$$X_2 = \frac{1}{2a_0}(-b_0 - \sqrt{b_0^2 - 4a_0c_0})$$

There is no real solution if $X_1 < 0$ or $X_2 < 0$, because we have to remember that X is actually the response amplitude squared ($X = a_q^2$). Therefore we need at least $X_1 > 0$ or $X_2 > 0$, or both. Then for that X value and its corresponding Y, we will have:

$$\begin{aligned} a_q &= \sqrt{X} \\ a_r &= \sqrt{Y} \end{aligned} \tag{5.8}$$

Once a_q and a_r are computed for each Y, we need to get the corresponding detuning parameter, σ, to be able to generate the a_q vs. σ, and a_r vs. σ, plots. So we first start by setting:

$$S = \sin\gamma$$

and

$$CC = \cos\gamma\ ,$$

and then we compute the following quantity using (5.2):

$$S = \frac{(B_{qq} - \xi_{qq}a_q^2 - \xi_{rq}a_r^2)a_q}{g_{rq}a_r} \tag{5.9}$$

If $S^2 > 1$, then we have no real solution; otherwise, we continue by finding:

$$\begin{aligned} CC &= +\sqrt{1 - S^2} \\ DD &= \frac{CC(g_{rq}Y - p_{qr}X)}{a_q a_r} \end{aligned} \tag{5.10}$$

and finally using (5.2), we get to:

$$\begin{aligned} \sigma_1 &= e_r - e_q + DD \\ \sigma_2 &= e_r - e_q - DD \end{aligned} \tag{5.11}$$

which are the detuning parameter values corresponding to a_q and a_r.

The stability of the solutions is checked using an IMSL subroutine called (DEVLRG) which computes the eigenvalues of a real, nonsymmetric matrix. For each

solution, a_r and a_q, we compute the following quantities called d_{ij}'s, which we then feed into the matrix program:

$$
\begin{aligned}
d_{11} &= -B_{qq} + 3\xi_{qq}a_q^2 + \xi_{rq}a_r^2 \\
d_{12} &= 2\xi_{rq}a_q a_r + g_{rq}\sin\gamma \\
d_{13} &= g_{rq}a_r\cos\gamma \\
d_{21} &= 2\xi_{qr}a_q a_r - p_{qr}\sin\gamma \\
d_{22} &= -B_{rr} + \xi_{qr}a_q^2 + 3\xi_{rr}a_r^2 \\
d_{23} &= -p_{qr}a_q\cos\gamma \\
d_{31} &= -\frac{\sigma}{a_q} - 2p_{qr}\frac{\cos\gamma}{a_r} \\
d_{32} &= -\frac{\sigma}{a_r} + 2g_{rq}\frac{\cos\gamma}{a_q} \\
d_{33} &= -g_{rq}\frac{a_r}{a_q}\sin\gamma + p_{qr}\frac{a_q}{a_r}\sin\gamma
\end{aligned}
\tag{5.12}
$$

The responses plotted in Figs. 5.1, 5.2, 5.3 and 5.4 of a_r vs. σ and a_q vs. σ are the results of increasing P from 0.25, to 0.35, to 0.5, then to unity. It is obvious that as the load amplitude increases, the response amplitudes a_q and a_r increase. There is a trivial solution at $a_q = 0$ and $a_r = 0$ that is always unstable, even between the bifurcation points. There are three different nontrivial solution curves when P is small, see Fig. 5.1. The solution curve near $a_q = 1$ corresponds to the solution curve with small values of a_r, and vice versa. The third nontrivial solution curve has two parts, a stable solution that begins at the vertical tangents, and an unstable solution below that.

In Fig. 5.2, the response increases as we increase the load amplitude, P. The solution curves with small values of a_q and with a_r close to unity have connected with the closed solution curves. Only a small portion at the top of this solution curve is stable. As

mentioned earlier, the trivial solution is unstable everywhere; the solution curve near $a_q = 1$ and the corresponding solution curve with small a_r are also unstable everywhere. The increase in the amplitude and the stable region is quite small compared to Fig. 5.1, but it still shows the effect the load has on the system response.

The load effect mentioned in the previous paragraph is more clear in Fig. 5.3 where the stable region spreads out more and the response amplitude is even higher. The vertical tangents disappear. Another difference from Fig. 5.2 is that the solution curve near $a_q = 1$ has a dip at the point of symmetry in the graph, or more precisely there is a sudden decrease in the response amplitude at about $\sigma = 2.5$. The solution curve close to zero has a sudden increase in the response amplitude at the same σ value.

Fig. 5.4 shows yet another aspect of the response as P is set equal to unity. The response amplitude is high, but the stable solutions in both a_q vs. σ and a_r vs. σ seem to be concentrated in a small area. This of course is not true, however; the difference is actually in the scale of the plots. From one figure to another in this chapter, the scale is only appropriate for the response shown on that specific graph. Therefore, as P increases, the amplitude of the response increases and so does the range of stable solutions. Another change occurring in Fig. 5.4 concerns the solution curves near $a_q = 1$ and $a_r = 0$. They both experience a sudden break in their curves, and the two independent parts hit $a_q = 0$ and $a_r = 0$, the trivial solution, in each case, at the values of the detuning parameter $\sigma \simeq 0$ and $\sigma \simeq 20$.

Also, if we examine the value of the detuning parameter, σ , about which each response is symmetric, $\sigma = e_r - e_q$. We see that this σ value increases as the load amplitude, P, increases. Actually the responses are symmetric about $\sigma \simeq 0.8$ in Fig. 5.1, then $\sigma \simeq 1.5$ in Fig. 5.2, $\sigma \simeq 2.5$ in Fig. 5.3, and $\sigma \simeq 11$ in Fig. 5.4.

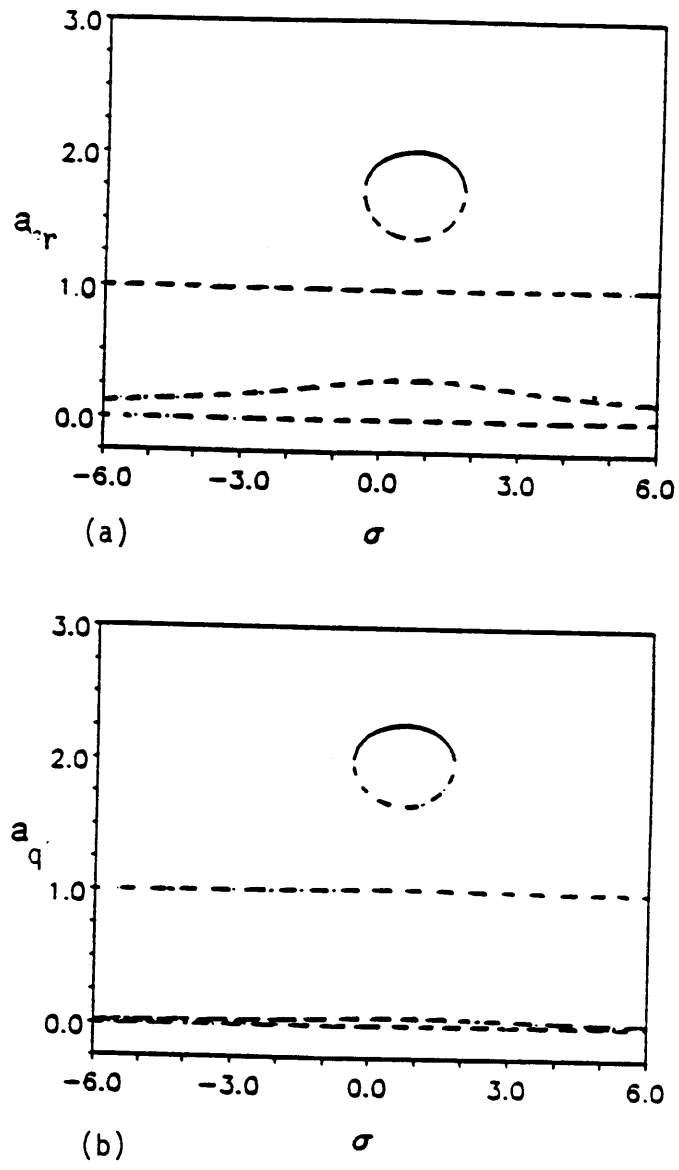

Figure 5.1. Frequency-Response Curves, (a) a_r vs. σ, (*b*) a_q vs. σ , where $P = 0.35$.

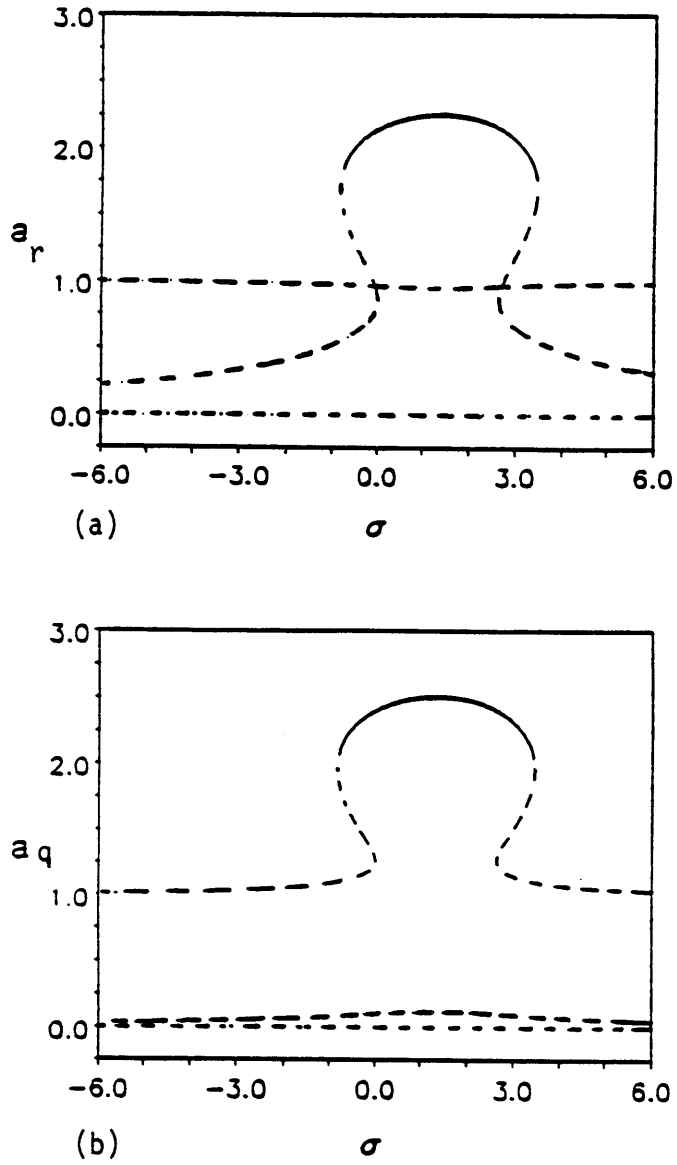

Figure 5.2. **Frequency-Response Curves,** (a) a_r vs. σ, (b) a_q vs. σ , where $P = 0.25$.

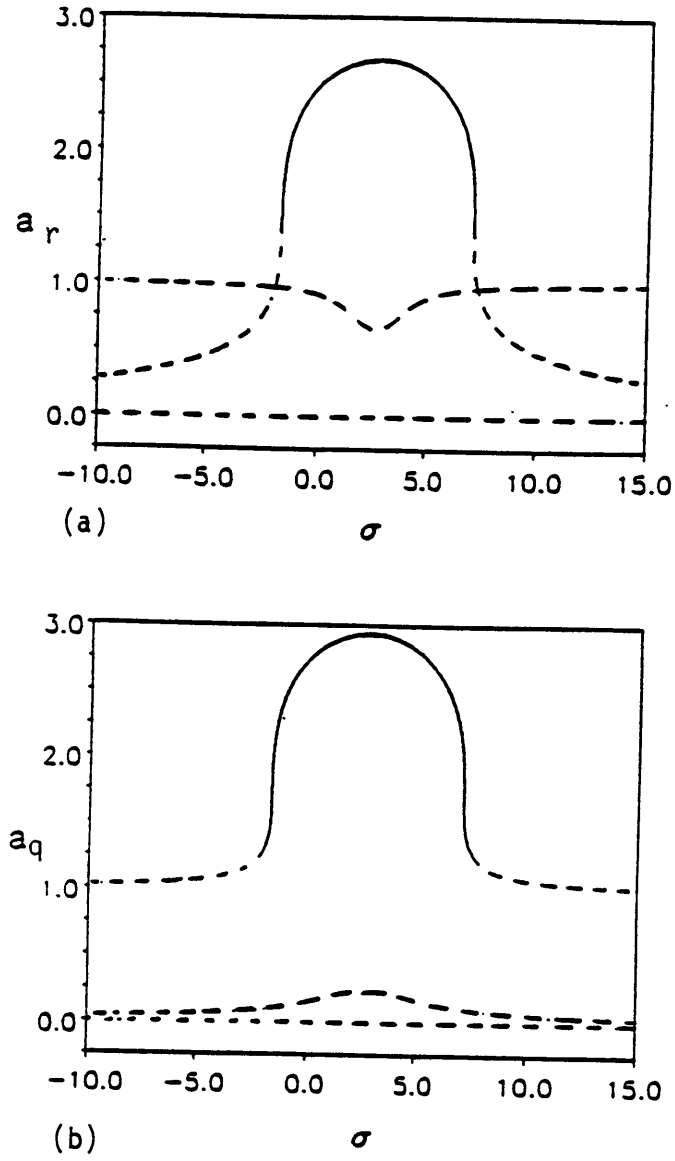

Figure 5.3. Frequency-Response Curves, (a) a_r vs. σ, (b) a_q vs. σ , where $P = 0.50$.

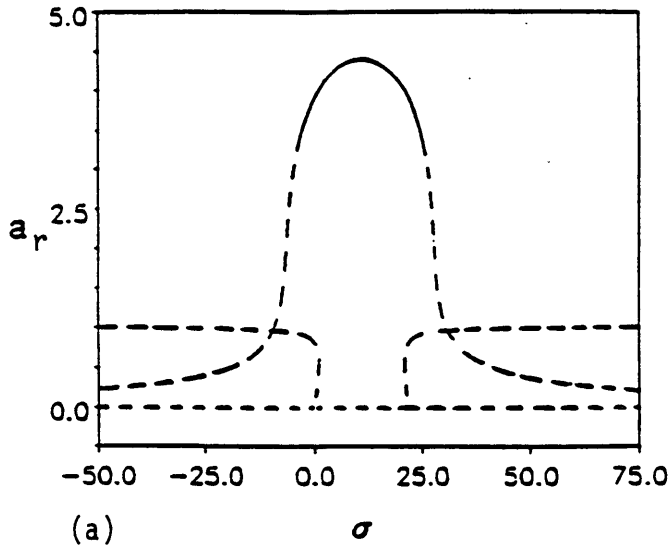

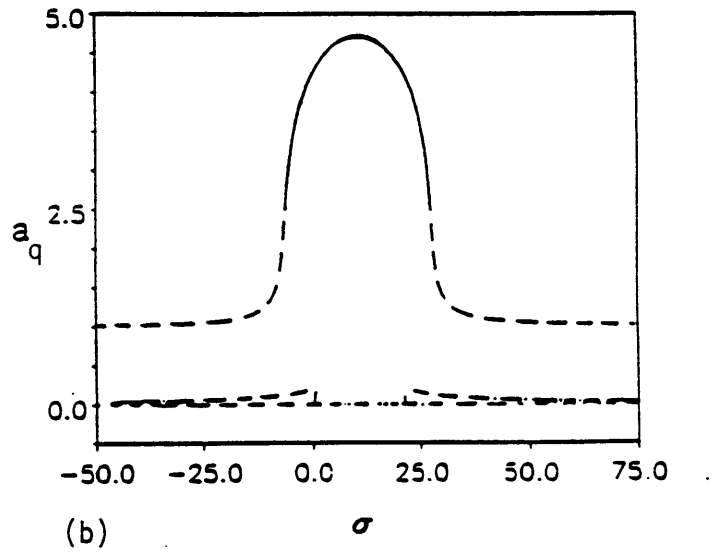

Figure 5.4. **Frequency-Response Curves,** (a) a_r vs. σ, (b) a_q vs. σ , where $P = 1.0$.

CHAPTER 6

CONCLUSION

In this study attention was focused on nonlinear oscillations under multifrequency parametric excitations. A system was chosen and different combinations of excitation frequencies and natural frequencies were analyzed. In all the previous studies, as mentioned in the literature review, many authors have taken interest in these types of behavior in a system. They have considered different systems and used different methods of solutions. Most of them focused on one case, when the excitation frequency is twice the natural frequency, $\lambda \simeq 2\omega$. This particular case was our first study case.

When $\lambda \simeq 2\omega$, the search started by finding the values, or the range of magnitudes, of the load amplitude, P, and the detuning parameter, σ, at which we get solutions.

These regions of existing solutions are then marked by I, II, and III in the P vs. σ plots. Afterwards, we check which ones are trivial, nontrivial, unstable, and stable; also we want to know, if there is a stable solution, in what interval of P and σ it stays stable. It is understood that our main concern in this study is to find stable solutions, and check all the different parameters that affect this state of stability in each case we treat. In the a vs. P plot, we vary P along the axis, and fix the detuning parameter, σ, and the stiffness value, α, for the different responses. We noticed that as the detuning parameter increases, the loads at which the nontrivial solutions became stable increased, and so did the bifurcation loads for the trivial ~~stable~~ solutions.

Still in case one, when the stiffness is nonlinear, $\alpha \neq 0$, and the system is perfectly tuned, $\sigma = 0$, we see the loads at which the solutions become stable increase. However, when $\sigma > 0$, then if the stiffness is positive, $\alpha = 1$, we have an increase in the loads, but the same is not true for $\alpha = -1$. The bifurcation loads in this case of nonlinear stiffness seem to be unaffected at all by the system stiffness; no matter what the sign of α is, the bifurcation load keeps the same magnitude. Next, we vary the detuning parameter, and fix the load amplitude. We see an increase in the response and therefore a larger range of stable nontrivial solutions as the load is increased. Examining the trivial solution, we also notice that when P is set higher, the trivial solution changes from being totally unstable everywhere to being stable between the bifurcation points. Another point to notice: when the stiffness is nonlinear, the response does not get any larger. However, since the solution gets deformed to the right and to the left depending on the sign of α, the range of the stable nontrivial solution seems to get slightly larger.

Case two deals with the parametric excitation frequency approximately equal to the natural frequency, $\lambda \simeq \omega$. This case has also been treated in a few studies. Again we begin

by checking the regions of existing solutions, and then we try to find the stable nontrivial and trivial ones. As we vary the detuning parameter, σ , and the load amplitude, P, we notice the response and the range of stability increasing with increasing P. The nontrivial solutions in this case are only stable above $a = \frac{1}{\sqrt{2}}$ and the vertical tangent of each solution curve, while the trivial solution is as usual stable between the bifurcation points. Then we go on and check the influence of the stiffness on the response and the stable solutions. When the stiffness is nonlinear, $\alpha \neq 0$, the number of stable nontrivial solutions increases with increasing load amplitudes. Finally, the influence of the detuning parameter, σ, on the system is checked. We find that as σ is increased, the load at which the nontrivial solution becomes stable increases, and the bifurcation load at which the trivial solution becomes stable increases, too.

In case three, we are interested in a single-degree-of-freedom system under two parametric excitation frequencies, with $\lambda_2 \pm \lambda_1 \simeq 2\omega$. As we can notice from the figures, we treated two sets of λ values, the first one: $\lambda_1 = 0.5$ and $\lambda_2 = 1.5$, the second set: $\lambda_1 = 0.5$ and $\lambda_2 = 2.5$. For each one of these two sets, we go through the same procedure for finding regions of existing solutions and the influence of the different parameters on the stable solutions. Once we find the regions where solutions exist, then we check the influence of the load amplitude, P, and the stiffness, α, on these solutions. We notice that as P gets larger the number of stable nontrivial solutions increases. The trivial solution is only stable when we have one nontrivial solution existing, while the nontrivial solution becomes stable at $a = \frac{1}{\sqrt{2}}$ and at the vertical tangent. Following that, we set $P_2 = 1$ and vary P_1 along the axis while changing the detuning parameter value, σ, for each response. When $|\sigma|$ is small the response and the number of stable nontrivial solutions is high; as $|\sigma|$ gets large the response disappears.

For the same case, we also investigate the effect of σ when we set $P_2 = P_1$. As seen in the other cases, the load at which the nontrivial solutions become stable are higher for $\sigma \neq 0$ and $\alpha > 0$ ($\alpha = 1$). ~~In this case the~~ trivial solution ~~becomes~~ stable at the ~~bi~~furcation point. Then we introduce a new variable Γ, which is actually a relationship between the two parametric excitations. For this variable, we checked the effect of the detuning parameter and the stiffness on the values of λ_1 and λ_2 at which stable trivial and nontrivial solutions exist. A reminder: in the figures dashed lines represent unstable solutions and solid lines imply stable solutions. For the same case of $\lambda_2 \pm \lambda_1 \simeq 2\omega$, we also introduce a second variable γ , and this one is a direct relationship of λ_2 and λ_1 ($\gamma = \frac{\lambda_1}{\lambda_2}$). Here, too, we investigate the effect of the detuning parameter, σ, and the stiffness parameter, α, on the existence of the stable solutions.

Case four deals with a two-degree-of-freedom system under two parametric excitation frequencies, with $\lambda_1 + \lambda_2 \simeq \omega_r - \omega_q$. We only checked the linear stiffness case due to time limitations. We generate the frequency-response curves as P is increased and examine the responses obtained. There are two different response amplitudes, a_q and a_r, and each one is plotted on a separate graph. If we go through the different figures in chapter 5 , it seems that the number of stable solutions is very scarce. The trivial solution is always unstable. Again the same checks are performed and as P increases, the response increases and most importantly, so does the number of stable nontrivial solutions.

Future research should include a numerical integration analysis. There are many more cases that we hope future studies will focus on. For example, one could try to investigate the effect of internal resonances on the system. Other topics could include the case of a multiple-degree-of-freedom system under multiple parametric excitation fre-

quencies, or two almost-equal parametric frequencies. Also, for a two-degree-of-freedom system under two parametric excitations, one could check the response of the system under different combinations of λ_i's and ω_i's other than the one discussed in chapter 5.

REFERENCE LIST

1. V. O. KONONENKO and P. S. KOVAL'CHUK 1971 *Soviet Applied Mechanics* 7, 583-589. The effect of parametric excitation on a self-oscillatory system.

2. V. O. KONONENKO and P. S. KOVAL'CHUK 1971 *Soviet Applied Mechanics* 7, 1061-1068. The effect of an external harmonic force on a self-excited oscillating system with a variable parameter.

3. A. TONDL 1978 *Monographs and Memoranda of the National Research Institute for Machine Design* Bechovice, Czechoslovakia, No. 25. On the interaction between self-excited and parametric vibrations.

4. A. H. NAYFEH and D. T. MOOK 1979 *Nonlinear Oscillations*, 342-343. New York, John Wiley & Sons.

5. S. YANO 1984 *Bulletin of the Japan Society of Mechanical Engineers* 27, 255-262. Parametric excitation in a self-excited vibration system with dry friction (1st report, parametric resonance).

6. S. YANO 1984 *Bulletin of the Japan Society of Mechanical Engineers* 27, 263-270. Parametric excitation in a self-excited vibration system with dry friction (2nd report, in the neighborhood of the region of parametric resonance).

7. S. YANO 1984 *Bulletin of the Japan Society of Mechanical Engineers* 27, 1264-1271. Parametric excitation in a self-excited vibration system (3rd report, the influence of cubic non-linearity).

8. S. YANO 1984 *Bulletin of the Japan Society of Mechanical Engineers* 27, 2483-2491. Parametric excitation in a self-exciting system (1st report, behaviors in the region of subharmonic resonance of order 1/2).

9. S. YANO 1985 *Bulletin of the Japan Society of Mechanical Engineers* 28, 483-491. Parametric excitation in a self-exciting system (2nd report, behaviors in the regions of resonances of order 1/3 and 2).

10. S. YANO 1985 *Bulletin of the Japan Society of Mechanical Engineers* 28, 671-678. Parametric excitation in a self-exciting system (4th report, region of subsuperharmonic resonance of order 2/3).

11. T. KOTERA and S. YANO 1985 *Bulletin of the Japan Society of Mechanical Engineers* 28, 1473-1480. Periodic solutions and the stability in a non-linear parametric excitation system.

12. S. YANO, T. KOTERA and T. HIRAMATSU 1986 *Bulletin of the Japan Society of Mechanical Engineers* 29, 902-907. Parametric excitation with an asymmetric

characteristic in a self-exciting system (1st report, behaviors of region of resonance of order 1/2).

13. S. YANO, T. KOTERA and T. HIRAMATSU 1986 *Bulletin of the Japan Society of Mechanical Engineers* 29, 3484-3490. Periodic solutions and the stability in a non-linear parametric excitation system (2nd report, consideration of solutions in the neighborhood of resonance of order 1).

14. G. SCHMIDT and A. TONDL 1986 *Non-linear Vibrations.* Cambridge: Cambridge University Press.

15. K. R. ASFAR 1980 *Response of Self-Excited Multidegree-of-Freedom Systems to Multifrequency Excitations.* Ph.D. dissertation, at Virginia Polytechnic Institute and State University, Blacksburg, Virginia.

16. F. WEIDENHAMMER 1981 *Zeitschrift fur angewandte Mathematik und Mechanik* 61, 633-638. Nicht-lineare Schwingungen mit fast-periodischer Parametererregung.

17. A. H. NAYFEH and A. E. S. JEBRIL 1987 *Journal of Sound and Vibration* 115, 83-101. The response of two-degree-of-freedom systems with quadratic and cubic non-linearities to multifrequency parametric excitations.

18. A. M. OTHMAN and D. WATT 1987 in *The Theory of Machines and Mechanisms* (editors, E. Bautista, J. Garcia-Lomas and A. Navarro). Oxford: Pergamon Press, 811-814. Response of an oscillator to multicomponent high frequency parametric excitation.

19. R. H. PLAUT to appear *International Journal of Non-Linear Mechanics.* Parametric excitation of an inextensible, air-inflated, cylindrical membrane.

20. R. H. PLAUT, J. J. GENTRY and D. T. MOOK to appear *International Journal of Non-Linear Mechanics.* Non-linear structural vibrations under combined multi-frequency parametric and external excitations. save

APPENDIX

The following equations are used in the different computations, in chapter 5.

$$\xi_{jn} = \frac{1}{4(1+\delta_{jn})}\left(C_{jjnn} + \omega_j^2(D_{jjnn} + D_{jnjn} + D_{njjn})\right) \tag{A1}$$

$$g_{rq} = 2\omega_q\left[R^t_{q\lambda r}P^s_{qq}P^t_{rq} + R^s_{q\lambda r}P^t_{qq}P^s_{rq} + R^t_{r\lambda r}P^s_{rq}P^t_{rr} + R^s_{r\lambda r}P^t_{rq}P^s_{rr}\right] \tag{A2}$$

$$p_{qr} = 2\omega_r\left[S^t_{q\lambda q}P^s_{qr}P^t_{qq} + S^s_{q\lambda q}P^t_{qr}P^s_{qq} + S^t_{r\lambda q}P^s_{rr}P^t_{qr} + S^s_{r\lambda q}P^t_{rr}P^s_{qr}\right] \tag{A3}$$

$$\begin{aligned} e_q = -2\big[&(R^s_{q\lambda q} + S^s_{q\lambda q})\omega_q(P^s_{qq})^2 + (R^t_{q\lambda q} + S^t_{q\lambda q})\omega_q(P^t_{qq})^2 \\ &+ (R^s_{r\lambda q} + S^s_{r\lambda q})\omega_r P^s_{rq}P^s_{qr} + (R^t_{r\lambda q} + S^t_{r\lambda q})\omega_r P^t_{rq}P^t_{qr}\big] \end{aligned} \tag{A4}$$

$$\begin{aligned} e_r = -2\big[&(R^s_{r\lambda r} + S^s_{r\lambda r})\omega_r(P^s_{rr})^2 + (R^t_{r\lambda r} + S^t_{r\lambda r})\omega_r(P^t_{rr})^2 \\ &+ (R^s_{q\lambda r} + S^s_{q\lambda r})\omega_q P^s_{qr}P^s_{rq} + (R^t_{q\lambda r} + S^t_{q\lambda r})\omega_q P^t_{qr}P^t_{rq}\big] \end{aligned} \tag{A5}$$

where

$$R^l_{i\lambda j} = \frac{1}{\omega_l^2 - (\lambda_l + \omega_j)^2} \tag{A6}$$

and

$$S^{l}_{iij} = \frac{1}{\omega_i^2 - (\lambda_l - \omega_j)^2} \tag{A7}$$

The vita has been removed from the scanned document